Available online at www.sciencedirect.com
SCIENCE DIRECT®
Journal of Magnetic Resonance 160 (2003) 166–182
JMR Journal of Magnetic Resonance
www.elsevier.com/locate/jmr

The continuous wave electron paramagnetic resonance experiment revisited

Moritz Kälin, Igor Gromov,[1] and Arthur Schweiger*

Physical Chemistry, ETH Zürich, CH-8093 Zürich, Switzerland

Received 3 September 2002; revised 18 October 2002

Abstract

When the modulation frequency used in continuous wave electron paramagnetic resonance (cw EPR) spectroscopy exceeds the linewidth, modulation sidebands appear in the spectrum. It is shown theoretically and experimentally that these sidebands are actually multiple photon transitions, $\sigma^+ + k \times \pi$, where one microwave (mw) σ^+ photon is absorbed from the mw radiation field and an arbitrary number k of radio frequency (rf) π photons are absorbed from or emitted to the modulation rf field. Furthermore, it is demonstrated that both the derivative shape of the lines in standard cw EPR spectra and the distortions due to overmodulation are caused by the unresolved sideband pattern of these lines. The single-photon transition does not even give a contribution to the first-harmonic cw EPR signal. Multiple photon transitions are described semiclassically in a toggling frame and their existence is proven using second quantization. With the toggling frame approach and perturbation theory an effective Hamiltonian for an arbitrary sideband transition is derived. Based on the effective Hamiltonians an expression for the steady-state density operator in the singly rotating frame is derived, completely describing all sidebands in all modulation frequency harmonics of the cw EPR signal. The relative intensities of the sidebands are found to depend in a very sensitive way on the actual rf amplitude and the saturation of single sidebands is shown to depend strongly on the effective field amplitude of the multiple photon transitions. By comparison with the analogous solutions for frequency-modulation EPR it is shown that the field-modulation and the frequency-modulation technique are not equivalent. The experimental data fully verify the theoretical predictions with respect to intensities and lineshapes.

PACS: 33.35.+r; 76.30.−v; 32.80.Wr

Keywords: Electron paramagnetic resonance; EPR; ESR; Multiple photon transitions; Modulation sidebands; Modulation broadening; Toggling frame

1. Introduction

Since the beginning of magnetic resonance spectroscopy modulation of the static magnetic field and phase-sensitive detection have been used to reduce the noise in measurements of weak continuous wave (cw) signals [1]. While in nuclear magnetic resonance (NMR) the cw technique has been replaced by pulsed techniques, it is still the most frequently used experimental method in electron paramagnetic resonance (EPR).

Due to modulation, cw EPR spectra can deviate from the derivative of the absorption spectrum predicted by the commonly used simple modulation theory. Distortions arise when the modulation amplitude or the modulation frequency are larger than the linewidth. In the latter case sidebands appear in the spectrum, which were explained classically by using modified Bloch equations [2]. Although the results describe the observed effects correctly, they give no insights into the physical process behind this phenomenon.

A first attempt to explain modulation-induced sidebands quantum mechanically was made by Miyagawa et al. [3]. Modulation-induced sidebands are also closely

* Corresponding author. Fax: +41-1-632-1021.
E-mail addresses: kaelin@phys.chem.ethz.ch (M. Kälin), gromov@phys.chem.ethz.ch (I. Gromov), schweiger@phys.chem.ethz.ch (A. Schweiger).
[1] On leave from MRS Laboratory, Kazan State University, 42008 Kazan, Russian Federation.

1090-7807/03/$ - see front matter © 2003 Elsevier Science (USA). All rights reserved.
doi:10.1016/S1090-7807(02)00186-6

related to the mechanisms behind double-modulation EPR, where two modulation frequencies are used; one frequency is kept constant and used for detection and the other frequency is varied [4].

In the so-called cw multi-quantum EPR spectroscopy [5–7], two or more microwave (mw) fields perpendicular to the static magnetic field are applied. Using many-mode Floquet theory [8,9] it was shown that the observed intermodulation sidebands of the mw frequencies are caused by absorption/emission processes of multiple mw photons [10]. Similar types of multiple photon transitions have been observed in cw NMR [11,12], as well as in pulse NMR [13–15], when two or four different rf fields are applied simultaneously. In EPR multiple photon transitions are involved in cw multi-quantum EPR experiments, double-quantum transition experiments in bimodal cavities [16–18] and single-mode cavities [19], and bichromatic pulse experiments [20,21], where mw and rf pulses were applied simultaneously.

Although the concept of multiple photon transitions was used to explain some special EPR experiments [22], it was not yet exploited to describe the processes behind modulation effects in conventional cw EPR spectroscopy. In this work, we first describe the classical approach to field modulation [2] and discuss a tilted rotating frame model used to explain multiple photon resonances [23]. Then a novel toggling frame approach is presented that is found to be best suited for the semiclassical description of field modulation. By using quantized radiation fields we prove that sidebands in cw EPR spectra are actually transitions where one mw σ^+ photon is absorbed and one or several rf π photons are absorbed or emitted. Using appropriate perturbation techniques an effective Hamiltonian describing the resonant transitions is derived. This effective Hamiltonian is found to be equivalent to the corresponding semiclassical toggling frame, as long as higher-order corrections are negligible. For weak mw amplitudes the solution is equivalent to the results derived with the tilted rotating frame approach. Furthermore, an answer is given to the often discussed question whether field modulation is equivalent to frequency modulation or not. The two techniques are found to be not equivalent, neither mathematically nor physically. The cw EPR spectrum recorded with the usual 100-kHz field modulation is found to consist of a large number of unresolved overlapping sidebands, corresponding to the absorption and emission of several dozens of rf photons. The calculated steady-state solution gives a complete description for any modulation frequency harmonics of the cw EPR signal and also describes distortions due to overmodulation. An interesting result is the fact that different sidebands show a different saturation behaviour. The theoretical findings are verified experimentally. EPR spectra of lithium phthalocyanine are measured at X- and Q-band with modulation frequencies up to several megacycles. The results are in good agreement with the theoretical predictions.

2. Theory

During a cw EPR experiment the Hamiltonian of an $S = 1/2$ electron spin system in the laboratory frame (in angular frequencies) is given by

$$\mathcal{H}_{\mathrm{lab}}(t) = \omega_{\mathrm{S}} S_z + 2\omega_1 \cos(\omega_{\mathrm{mw}} t) S_x + 2\omega_2 \times \cos(\omega_{\mathrm{rf}} t) S_z, \tag{1}$$

with the Larmor frequency $\omega_{\mathrm{S}} = \gamma_e B_0 = g_e \mu_B B_0/\hbar$ of the electron spin, the linearly polarized mw field $2\omega_1 \cos(\omega_{\mathrm{mw}} t)$ with amplitude $2\omega_1 = \gamma_e B_{\mathrm{mw}}$ perpendicular and the linearly polarized modulation field $2\omega_2 \cos(\omega_{\mathrm{rf}} t)$ with amplitude $2\omega_2 = \gamma_e B_{\mathrm{rf}}$ parallel to the static magnetic field $\mathbf{B}_0$.

After transformation to a frame rotating with ω_{mw} around the z axis and after omitting the counter-rotating part of the mw field, one gets

$$\mathcal{H}_{\mathrm{SRF}}(t) = \Omega_{\mathrm{S}} S_z + \omega_1 S_x + 2\omega_2 \cos(\omega_{\mathrm{rf}} t) S_z, \tag{2}$$

with the resonance offset $\Omega_{\mathrm{S}} = \omega_{\mathrm{S}} - \omega_{\mathrm{mw}}$. These two Hamiltonians are the starting point for all semiclassical and quantum-mechanical calculations in this work.

2.1. Semiclassical description

Modulation can be described by semiclassical models with varying degree of complexity. In this section two existing approaches will be briefly discussed and a new toggling frame will be introduced.

2.1.1. Modified Bloch equations

A first description of modulation effects was given by Karplus [24] for mw rotational spectroscopy, where either the excitation frequency or the energy levels of the molecule are modulated (Stark effect). In magnetic resonance this theory was first used by Smaller [25] and was further developed to obtain quasi steady-state solutions of the modified Bloch equations [2,26–29].

Magnetic resonance phenomena of ensembles of non-interacting $S = 1/2$ spins can be described classically by their magnetization. The behaviour of the magnetization vector $\mathbf{M} = (M_x, M_y, M_z)$ under the influence of a static and an oscillatory magnetic field is described by the Bloch equations [30]. The semiclassical analogue of the Bloch equations is the master equation in Liouville space [31]

$$\frac{\mathrm{d}}{\mathrm{d}t}\boldsymbol{\sigma} = -\mathrm{i}\mathbf{H}\boldsymbol{\sigma} - \boldsymbol{\Gamma}(\boldsymbol{\sigma} - \boldsymbol{\sigma}_0), \tag{3}$$

with the density operator $\boldsymbol{\sigma} = (\{\sigma\}_x, \{\sigma\}_y, \{\sigma\}_z)$ in vector form, the commutator superoperator $\mathbf{H}$, the relaxation superoperator $\boldsymbol{\Gamma}$, and the density operator $\boldsymbol{\sigma}_0 = (0, 0, -1)$ at thermal equilibrium.

A convenient choice for a basis system in Liouville space is (S_x, S_y, S_z), which allows for a simple relation between the density operator and the magnetization vector, $M_q = 2\,\mathrm{tr}\{\sigma S_q\}M_0$, with $q = x, y, z$. For the Hilbert space Hamiltonian in the rotating frame, $\mathcal{H} = \Omega_S S_z + \omega_1 S_x$, the master equation in matrix form is then given by

$$\frac{\mathrm{d}}{\mathrm{d}t}\boldsymbol{\sigma} = -\mathrm{i}\begin{pmatrix} & -\Omega_S & \\ \Omega_S & & \omega_1 \\ & -\omega_1 & \end{pmatrix}\boldsymbol{\sigma} - \begin{pmatrix} 1/T_2 & & \\ & 1/T_2 & \\ & & 1/T_1 \end{pmatrix}(\boldsymbol{\sigma} - \boldsymbol{\sigma}_0). \tag{4}$$

The resonance offset can either be constant, $\Omega_S = \omega_S - \omega_{mw}$, or time dependent due to field (or frequency) modulation $\Omega_S(t) = \omega_S - \omega_{mw} + 2\omega_2\cos(\omega_{rf}t)$. T_1 and T_2 are the phenomenological longitudinal and transverse relaxation times, respectively.

For a *time-independent Hamiltonian* the solution of the differential equations for $\mathrm{d}\boldsymbol{\sigma}/\mathrm{d}t = 0$ gives the steady-state density operator $\boldsymbol{\sigma}^{ss}$. The dispersion signal is given by the component in-phase with the mw irradiation

$$\{\sigma^{ss}\}_x = -\frac{\Omega_S\omega_1 T_2^2}{(1+\omega_1^2 T_1 T_2) + \Omega_S^2 T_2^2} \tag{5}$$

and the absorption signal by the out-of-phase component

$$\{\sigma^{ss}\}_y = \frac{\omega_1 T_2}{(1+\omega_1^2 T_1 T_2) + \Omega_S^2 T_2^2}. \tag{6}$$

To find a steady-state solution for the density operator under a *time-dependent Hamiltonian* one assumes that the modulation frequency is slow compared to the relaxation rates. The time-dependent steady-state is then calculated in analogy to the time-independent case. The solution of this modified master equation derived from the Hamiltonian in Eq. (2) for $\mathrm{d}\boldsymbol{\sigma}/\mathrm{d}t = 0$ consists of constants, periodic terms with multiples of the modulation frequency, and exponentially decaying terms. Since we are only interested in the steady-state solution, the exponential terms are neglected. For negligible saturation $(\omega_1^2 T_1 T_2 \ll 1)$ the absorption component was found to be [2,28]

$$\{\sigma^{ss}\}_y = \sum_{n=-\infty}^{\infty}\sum_{k=-\infty}^{\infty}\omega_1 J_n\left(\frac{2\omega_2}{\omega_{rf}}\right)J_{-k}\left(\frac{2\omega_2}{\omega_{rf}}\right) \times \frac{T_2\cos([k+n]\omega_{rf}t) - (\Omega_S - k\omega_{rf})T_2^2\sin([k+n]\omega_{rf}t)}{1+(\Omega_S - k\omega_{rf})^2 T_2^2}, \tag{7}$$

with the Bessel functions $J_v(z)$ of the first kind. The phase change due to the different signs of ω_1 in EPR and proton NMR is canceled by the phase change due to the reversed thermal equilibrium polarization ($-S_z$ in EPR vs. I_z in proton NMR). Eq. (7) thus can be used for proton NMR and EPR without sign corrections. Compared to the original formula in [2] indices n and k are interchanged for compatibility with our results.

In principle Eq. (7) allows for a full description of all phenomena related to magnetic field modulation. Nevertheless, it is derived from the phenomenological semiclassical master equation and gives no insight into the real physical processes involved.

2.1.2. Multiply tilted rotating frames

Another approach to treat the effects of an rf field parallel to the static magnetic field and to explain the existence of sidebands makes use of a frame that is obtained by a succession of transformations. Each transformation consists of a rotation and a subsequent transformation to a rotating frame [20,23]. In contrast to the approach based on the modified Bloch equations this multiply tilted rotating frame model has the advantage of being also applicable to pulse experiments.

The Hamiltonian in the singly rotating frame in Eq. (2) is shown graphically in Fig. 1a. The effective nutation frequency vector $\boldsymbol{\omega}_{\mathbf{eff}}$ is tilted from the z axis by the angle $\alpha = \arctan(\omega_1/\Omega_S)$. The modulation field thus has a component perpendicular to $\boldsymbol{\omega}_{\mathbf{eff}}$. The frame is then tilted around the y axis by the angle α, resulting in a new z' axis parallel to $\boldsymbol{\omega}_{\mathbf{eff}}$. Finally, the new frame is transformed

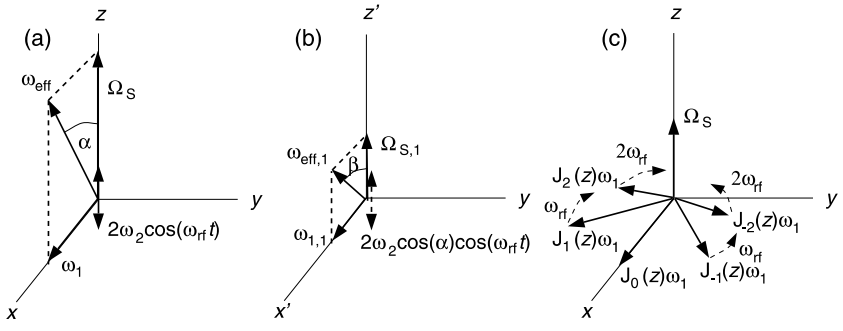

Fig. 1. Pictorial representation of the cw EPR Hamiltonian in (a) the singly rotating frame, (b) the first tilted rotating frame, tilted from the original z axis by the angle α and rotating with ω_{rf}. β gives the tilt angle for the next transformation, (c) a toggling frame with $k = 0$ and $z = 2\omega_2/\omega_{rf}$, according to Eq. (22).

to a frame rotating with frequency ω_{rf}. The resulting Hamiltonian is shown in Fig. 1b.

In this doubly rotating frame the magnetization at thermal equilibrium, oriented along the z axis in the singly rotating frame, lies on a cone with an apex angle 2α. The position on the cone depends on the rf phase. For small angles α, corresponding to $\omega_1 \ll \Omega_S$, the magnetization can be assumed to lie approximately parallel to the z' axis.

The resulting Hamiltonian, after omitting the counter-rotating term and the remaining linearly polarized component, is given by

$$\mathcal{H}_{TRF,1} = \Omega_{S,1} S_z + \omega_{1,1} S_x. \tag{8}$$

The new resonance offset is defined as $\Omega_{S,1} = \omega_{eff} - \omega_{rf} = \sqrt{\omega_1^2 + \Omega_S^2} - \omega_{rf} \approx \Omega_S - \omega_{rf}$. For the effective field amplitude $\omega_{1,1}$ in the first tilted rotating frame we find

$$\omega_{1,1} = -\omega_2 \sin(\alpha) = \frac{-\omega_1\omega_2}{\sqrt{\omega_1^2 + \Omega_S^2}} = \frac{-\omega_1\omega_2}{\Omega_{S,1} + \omega_{rf}}, \tag{9}$$

which near resonance ($\Omega_{S,1} \ll \omega_{rf}$) can be simplified to

$$\omega_{1,1} \approx \frac{-\omega_1\omega_2}{\omega_{rf}}, \tag{10}$$

leading to the Hamiltonian

$$\mathcal{H}_{TRF,1} = (\Omega_S - \omega_{rf}) S_z - \frac{\omega_1\omega_2}{\omega_{rf}} S_x. \tag{11}$$

This Hamiltonian describes a transition resonant for $\Omega_S = \omega_{rf}$, corresponding in a field-swept experiment to a sideband at higher field. It implies the idea of a two-photon transition process.

For the second sideband the procedure is similar. Starting from the Hamiltonian in Eq. (8) a new effective nutation vector with amplitude $\omega_{eff,1} = [\omega_{1,1}^2 + \Omega_{S,1}^2]^{1/2}$ is defined, tilted from the z' axis by the angle $\beta = \arctan(\omega_{1,1}/\Omega_{S,1})$, as it is shown in Fig. 1b. The frame is tilted by β and again transformed to a frame rotating with ω_{rf}. The Hamiltonian in this triply rotating frame is then

$$\mathcal{H}_{TRF,2} = \Omega_{S,2} S_z + \omega_{1,2} S_x, \tag{12}$$

with $\Omega_{S,1} = \omega_{eff,1} - \omega_{rf} \approx \Omega_S - 2\omega_{rf}$. For the effective field amplitude we find

$$\omega_{1,2} = -\omega_2 \sin(\beta)\cos(\alpha) \approx \frac{\omega_1\omega_2^2}{2\omega_{rf}^2} \sqrt{1 - \left(\frac{\omega_1}{2\omega_{rf}}\right)^2}. \tag{13}$$

For small mw amplitudes, $\omega_1 \ll 2\omega_{rf}$, Eq. (13) can be further simplified to

$$\omega_{1,2} \approx \frac{\omega_1\omega_2^2}{2\omega_{rf}^2}, \tag{14}$$

so that

$$\mathcal{H}_{TRF,2} = (\Omega_S - 2\omega_{rf}) S_z + \frac{\omega_1\omega_2^2}{2\omega_{rf}^2} S_x. \tag{15}$$

By repeating this procedure the Hamiltonian for any sideband resonance is obtained.

For larger amplitudes of the mw and rf radiation fields, the used approximations and the multiply tilted rotating-frame model fail to explain the observed effects. To describe multiple photon transitions in a more general way, a more suitable model has to be used.

2.1.3. Toggling frame

To simplify the calculations we introduce the toggling frame, a kind of a generalized rotating frame. We will demonstrate that the toggling frame is very convenient for the description of $\sigma^+ + k \times \pi$ transitions. The first step, the transformation of the laboratory frame to a frame rotating with frequency ω_{mw} is straightforward, since all discussed multiple photon transitions will include the absorption of one mw σ^+ photon. In a second step all time-dependent S_z components in the Hamiltonian are removed and replaced by time-dependent transverse components. For this purpose an appropriate rotation operator defining such a transition is introduced.

A general rotation operator can be written as $R(t) = \exp(-i\alpha q)$, with the rotation angle α and the normalized spin operator q defining the rotation axis in the Hilbert space.

The Liouville–von Neumann equation, $d\sigma/dt = -i[\mathcal{H}, \sigma]$, is also valid in the new frame, which leads to

$$\mathcal{H}'(t) = R(t)\mathcal{H}R^{-1}(t) + \frac{d\alpha(t)}{dt} q. \tag{16}$$

We now choose an appropriate function $\alpha(t)$ which removes the S_z component in $\mathcal{H}'(t)$. For a time-independent rotation frequency ω, the rotation angle is $\alpha = -\omega t$ and the rotation axis operator $q = S_z$, leading to the well-known solution for the rotating frame, $\mathcal{H}' = R\mathcal{H}R^{-1} - \omega S_z$.

For the Hamiltonian in Eq. (2) the condition

$$\frac{d\alpha(t)}{dt} q = -[\Omega_S + 2\omega_2 \cos(\omega_{rf} t)] S_z \tag{17}$$

has to be fulfilled, which leads to $q = S_z$ and

$$\alpha(t) = -k\omega_{rf} t - \left(\frac{2\omega_2}{\omega_{rf}}\right) \sin(\omega_{rf} t), \tag{18}$$

and thus to the rotation operator

$$R(t) = \exp\left\{ i\left[k\omega_{rf} t + \left(\frac{2\omega_2}{\omega_{rf}}\right) \sin(\omega_{rf} t)\right] S_z \right\}. \tag{19}$$

The parameter k can have any value, $k \in \mathbb{Z}_0$. One possible choice is a value that minimizes the resonance offset in the toggling frame. As will be shown later, this corresponds to the resonance condition of the kth sideband, respectively, its corresponding multiple photon transition $\sigma^+ + k \times \pi$.

With the relation [32]

$$e^{iz\sin(\theta)} = \sum_{n=-\infty}^{+\infty} J_n(z)e^{in\theta} \tag{20}$$

and the expression

$$\exp(iAtS_z)S_x\exp(-iAtS_z) = (1/2)S^+\exp(iAt) + (1/2)S^-\exp(-iAt), \tag{21}$$

which is analogously valid for S_y, the toggling-frame Hamiltonian is found to be

$$\begin{aligned}\mathcal{H}_{TF,k} &= R(t)\mathcal{H}_{SRF}R^{-1}(t) - k\omega_{rf}S_z - 2\omega_2 \times \cos(\omega_{rf}t)S_z \\ &= (\Omega_S - k\omega_{rf})S_z \\ &\quad + \sum_{n=-\infty}^{+\infty}\omega_1 J_n\left(\frac{2\omega_2}{\omega_{rf}}\right)\left[\frac{1}{2}e^{i(k+n)\omega_{rf}t}S^+ + \frac{1}{2}e^{-i(k+n)\omega_{rf}t}S^-\right] \\ &= (\Omega_S - k\omega_{rf})S_z + J_{-k}\left(\frac{2\omega_2}{\omega_{rf}}\right)\omega_1 S_x \\ &\quad + \sum_{n=-\infty, n\neq -k}^{+\infty} J_n\left(\frac{2\omega_2}{\omega_{rf}}\right)\omega_1 e^{i(k+n)\omega_{rf}tS_z}S_x e^{-i(k+n)\omega_{rf}tS_z},\end{aligned} \tag{22}$$

$\mathcal{H}_{TF,k}$ contains the resonance offset $(\Omega_S - k\omega_{rf})$, a constant effective field amplitude $J_{-k}(2\omega_2/\omega_{rf})\omega_1$, and the sum of time-dependent perturbations. For a better understanding $\mathcal{H}_{TF}$ is shown in Fig. 1c for $k = 0$. The component $J_0(2\omega_2/\omega_{rf})\omega_1$ points along the x axis while all other transverse components rotate with multiples of ω_{rf} around the z axis. If the value for k is properly chosen, so that the remaining resonance offset is minimum, the time-dependent terms of the Hamiltonian can be omitted in a first-order approximation. $J_{-k}(2\omega_2/\omega_{rf})\omega_1$ may now be interpreted as the effective field amplitude of a $\sigma^+ + k \times \pi$ multiple photon transition.

Although the toggling frame is a very convenient tool for understanding multiple photon processes, it remains a *semiclassical* description. In the next section, we use a quantized electromagnetic radiation field to prove mathematically the existence of multiple photon transitions.

2.2. Quantum mechanical description

2.2.1. Multiple photon transitions

Since transitions in quantum systems must follow the conservation of energy and angular momentum, the total angular momentum of the radiation field and the spin system has to be constant. For single-photon transitions this leads to the selection rule $\Delta m = \pm 1$.

Photons have an angular momentum quantum number $J = 1$ and a helicity (projection of the angular momentum on the direction of propagation) of $m_J = \pm 1$. The corresponding eigenfunctions are called σ^- and σ^+, and refer to left- and right-hand circularly polarized photons [33]. The photon wavefunction $\pi = (\sqrt{2}/2)\sigma^+ + (\sqrt{2}/2)\sigma^-$ describes a linearly polarized π photon with no angular momentum.

A standing electromagnetic wave in a cavity formed by σ^+ photons results in a right-hand rotating electromagnetic field (respectively left-hand for σ^- photons). A linearly polarized field can be considered as a superposition of a left- and a right-hand circularly polarized field respectively as a standing electromagnetic wave formed by π photons.

The linearly polarized mw radiation field perpendicular to $\mathbf{B}_0$ is formed by photons propagating parallel to the direction of $\mathbf{B}_0$. Consequently, their angular momentum vector is also oriented parallel to $\mathbf{B}_0$. The linearly polarized modulation rf field is oriented parallel to the static magnetic field and is formed by a standing wave of photons propagating perpendicular to $\mathbf{B}_0$, with their angular momentum also perpendicular to $\mathbf{B}_0$.

Since the spin system is quantized along $\mathbf{B}_0$, only σ photons are absorbed from or emitted to the mw field during a transition, whereas for the rf field only π photons can be absorbed or emitted. A transition with $\Delta m = 1$ can then include the absorption of one mw σ^+ photon and the absorption or emission of an arbitrary number k of rf π photon. Transitions like $\sigma^+ + \sigma^- + \sigma^+$ may also occur, but they are far off-resonant and of no interest for our considerations.

2.2.2. Quantized radiation field and Floquet theory

The relation between photons and radiation fields is described by the second quantization approach, where the classical electromagnetic radiation field is considered as a set of quantized harmonic oscillators, which are then included in the Hamiltonian [33–36].

A similar approach has already been used in a study of double-modulation EPR [37].

The complete Hamiltonian is given by

$$\mathcal{H} = \mathcal{H}_S + \mathcal{H}_R + \mathcal{H}_i, \tag{23}$$

with the Hamiltonian $\mathcal{H}_S$ of the undisturbed spin system, the Hamiltonian $\mathcal{H}_R$ of the radiation field, and the interaction Hamiltonian $\mathcal{H}_i$, describing the coupling between spin system and radiation field.

In a cavity the electromagnetic field is represented by the superposition of all possible modes of radiation. The different modes are orthogonal and do not interact with each other. The Hamiltonian representing the radiation field is given by

$$\mathcal{H}_R = \sum_k \omega_k\left(a_k^T a_k + \frac{1}{2}\right), \tag{24}$$

with the photon energy ω_k and the annihilation and creation operators a_k and a_k^T. The eigenfunctions of a mode k are $|n_k\rangle_k$, representing the presence of n_k photons with energy ω_k.

The laboratory-frame Hamiltonian of the cw EPR experiment in Eq. (1) consists of two modes with frequencies ω_{mw} and ω_{rf}. The spatial orientation of the radiation fields does not enter in $\mathcal{H}_{\mathrm{R}}$, since it has no relation to the energy. It however influences the coupling to the spin system. The state function of a single mode, defined by

$$a|\alpha\rangle = \alpha|\alpha\rangle, \tag{25}$$

is called a *coherent state*, given by

$$|\alpha\rangle = \sum_{n=0}^{\infty} \mathrm{e}^{-\frac{1}{2}|\alpha|^2} \frac{\alpha^n}{\sqrt{n!}} |n\rangle. \tag{26}$$

The populations of the different levels follow a Poisson distribution

$$|\langle n|\alpha\rangle|^2 = \mathrm{e}^{|\alpha|^2} \frac{\alpha^{2n}}{n!}, \tag{27}$$

with the average photon number $N = \alpha_2$, which for the low frequencies used in magnetic resonance is very large. The exact value can be estimated from the energy stored in the cavity.

In a cw EPR experiment only the mw and the rf mode are of importance. All modes with other frequencies are either strongly damped or far off-resonant. The overall coherent state in the cw EPR experiment is then

$$|\Psi\rangle = |\alpha\rangle_{\mathrm{mw}}|\beta\rangle_{\mathrm{rf}}. \tag{28}$$

The interaction Hamiltonian in the semiclassical form is given by

$$\mathcal{H}_{\mathrm{i,semicl}} = 2\omega_1 \cos(\omega_{\mathrm{mw}} t) S_x + 2\omega_2 \cos(\omega_{\mathrm{rf}} t) S_z, \tag{29}$$

and its quantized counter-part is

$$\mathcal{H}_{i,\mathrm{quant}} = \lambda_{\mathrm{mw}}(a_{\mathrm{mw}}^{\mathrm{T}} + a_{\mathrm{mw}}) S_x + \lambda_{\mathrm{rf}}(a_{\mathrm{rf}}^{\mathrm{T}} + a_{\mathrm{rf}}) S_z, \tag{30}$$

with the coupling constants λ_{mw} and λ_{rf}. The two Hamiltonians have to be equal, $\mathcal{H}_{\mathrm{i,quant}} = \mathcal{H}_{\mathrm{i,semicl}}$, so that

$$\lambda_{\mathrm{mw}} = \frac{\omega_1}{\sqrt{N_{\mathrm{mw}}}} \quad \text{and} \quad \lambda_{\mathrm{rf}} = \frac{\omega_2}{\sqrt{N_{\mathrm{rf}}}}. \tag{31}$$

The complete and fully quantized Hamiltonian is then given by

$$\begin{aligned} \mathcal{H} &= \mathcal{H}_{\mathrm{S}} + \mathcal{H}_{\mathrm{R}} + \mathcal{H}_{\mathrm{i,quant}} \\ &= \omega_{\mathrm{S}} S_z + \omega_{\mathrm{mw}} \left(a_{\mathrm{mw}}^{\mathrm{T}} a_{\mathrm{mw}} + \frac{1}{2} \right) + \omega_{\mathrm{rf}} \left(a_{\mathrm{rf}}^{\mathrm{T}} a_{\mathrm{rf}} + \frac{1}{2} \right) \\ &\quad + \frac{\omega_1}{\sqrt{N_{\mathrm{mw}}}} (a_{\mathrm{mw}}^{\mathrm{T}} + a_{\mathrm{mw}}) S_x + \frac{\omega_2}{\sqrt{N_{\mathrm{rf}}}} (a_{\mathrm{rf}}^{\mathrm{T}} + a_{\mathrm{rf}}) S_z. \end{aligned} \tag{32}$$

Its function space is spanned by $|m_{\mathrm{S}}, n, m\rangle = |m_{\mathrm{S}}\rangle \otimes |n\rangle \otimes |m\rangle$, where n and m are the numbers of mw and rf photons in the modes.

For very high average photon numbers the Poisson distribution approximates a Gaussian distribution and almost exclusively states with $n \approx N_{\mathrm{mw}}$ and $m \approx N_{\mathrm{rf}}$ are populated. For these the coupling terms $\langle m_{\mathrm{S}}, n, m|\mathcal{H}_{\mathrm{i,quant}}| -m_{\mathrm{S}}, n+1, m\rangle$ and $\langle m_{\mathrm{S}}, n, m|\mathcal{H}_{\mathrm{i,quant}}|m_{\mathrm{S}}, n, m+1\rangle$ are in good approximation equal to $(1/2)\omega_1$ and $(1/2)\omega_2$. The quantized field Hamiltonian can then be replaced by a Hamiltonian in Floquet space [38–40],

$$\mathcal{H}_{\mathrm{F}} = \mathcal{H} - \left[\left(N_{\mathrm{mw}} + \frac{1}{2} \right) \omega_{\mathrm{mw}} + \left(N_{\mathrm{rf}} + \frac{1}{2} \right) \omega_{\mathrm{rf}} \right] \mathbf{1}. \tag{33}$$

The Floquet Hamiltonian is basically a semiclassical Hamiltonian, in which the spin system is considered to be *dressed* by an arbitrary number of photons. The advantages of the Floquet approach compared to the quantized field approach are the reduced number of considered photons (only differences of photon numbers are of interest) and the simpler back-transformation to Hilbert space. Since the Floquet Hamiltonian derived from Eq. (33) contains two modes of radiation, many-mode Floquet theory, an expanded version of the Floquet theory, has to be used [8,9]. The corresponding function space is spanned by the functions $|m_{\mathrm{S}}, n', m'\rangle$ with $n', m' = -\infty, \ldots, \infty$. The condition for a multiple photon resonance of the type $\sigma_{\mathrm{mw}}^{+} + k \times \pi_{\mathrm{rf}}$ between two levels $\langle \alpha, 0, 0|$ and $\langle \beta, 1, k|$ of a Hamiltonian in Floquet space is fulfilled when $\langle \alpha, 0, 0|\mathcal{H}_{\mathrm{F}}|\alpha, 0, 0\rangle \approx \langle \beta, 1, k|\mathcal{H}_{\mathrm{F}}|\beta, 1, k\rangle$. Coupling between the degenerate levels will then lead to a coherent transition in the form of Rabi oscillations.

The main difference between the Floquet/quantized-field description and the semiclassical description is that in the quantized-field approach the photon absorption and emission process is clearly defined as a transition between two degenerate levels. It therefore allows one to prove that the modulation sidebands are actually multiple photon transitions.

When transient effects are investigated the evolution of the density operator in Hilbert space can be calculated numerically from the Floquet Hamiltonian [41]. In the case of cw EPR only the steady-state solution is of interest. An analytical approximation is obtained by singling out the resonant submatrices using appropriate perturbation techniques.

2.2.3. Perturbative approximation

If two arbitrary energy levels $\langle q|$ and $\langle p|$ of a Hamiltonian are nearly degenerate, an effective Hamiltonian in a two-dimensional subspace can be constructed using perturbation theory methods [13,20,42]. The diagonal elements are given by

$$\langle q|\mathcal{H}_{\mathrm{eff}}|q\rangle = \langle q|\mathcal{H}_{\mathrm{F}}|q\rangle + \Delta(q), \tag{34}$$

$$\langle p|\mathcal{H}_{\mathrm{eff}}|p\rangle = \langle p|\mathcal{H}_{\mathrm{F}}|p\rangle + \Delta(p). \tag{35}$$

The higher-order perturbation corrections $\Delta(p), \Delta(q)$ which include the contributions of the terms of the neglected Hamiltonian elements in the complementary subspace are calculated by

$$\Delta(p) = \sum_{r\neq q,p} \frac{\langle p|\mathcal{H}_F|r\rangle\langle r|\mathcal{H}_F|p\rangle}{\langle p|\mathcal{H}_F|p\rangle - \langle r|\mathcal{H}_F|r\rangle} + \sum_{r,k\neq q,p} \frac{\langle p|\mathcal{H}_F|r\rangle\langle r|\mathcal{H}_F|k\rangle\langle k|\mathcal{H}_F|p\rangle}{[\langle p|\mathcal{H}_F|p\rangle - \langle r|\mathcal{H}_F|r\rangle][\langle p|\mathcal{H}_F|p\rangle - \langle k|\mathcal{H}_F|k\rangle]} + \cdots \quad (36)$$

The two anti-diagonal elements, expressing the effective coupling between the two degenerate levels, are given by

$$\langle p|\mathcal{H}_{\text{eff}}|q\rangle = \langle p|\mathcal{H}_F|q\rangle + \frac{1}{2}\omega(p;q), \quad (37)$$

and

$$\langle q|\mathcal{H}_{\text{eff}}|p\rangle = \langle p|\mathcal{H}_{\text{eff}}|q\rangle^*. \quad (38)$$

For the higher-order terms we find

$$\omega(p;q) = 2\sum_{r\neq q,p} \frac{\langle p|\mathcal{H}_F|r\rangle\langle r|\mathcal{H}_F|q\rangle}{\langle p|\mathcal{H}_F|p\rangle - \langle r|\mathcal{H}_F|r\rangle} + 2\sum_{r,k\neq q,p} \frac{\langle p|\mathcal{H}_F|r\rangle\langle r|\mathcal{H}_F|k\rangle\langle k|\mathcal{H}_F|q\rangle}{[\langle p|\mathcal{H}_F|p\rangle - \langle r|\mathcal{H}_F|r\rangle][\langle p|\mathcal{H}_F|p\rangle - \langle k|\mathcal{H}_F|k\rangle]} + \cdots \quad (39)$$

Fig. 2a shows a segment of the two-mode Floquet Hamiltonian in Eq. (33). The two levels $|\alpha,0,0\rangle$ and $|\beta,1,1\rangle$ are degenerate, corresponding to the two-photon transition $\sigma^+ + \pi$. Since there is no direct coupling between the elements, only second-order (two-photon transitions) and higher-order effects take place. The two different pathways for the two-photon transition are indicated by arrows and correspond to the transitions (I) and (II) in Fig. 2b. By using Eq. (39) the contribution of these two pathways to the coupling element is found to be $(-\omega_1\omega_2/\omega_{\text{rf}})$. The next possible transition pathways are the four-photon transitions $-\sigma^+ + \pi + 2\sigma^+$, $2\sigma^+ + \pi - \sigma^+$, $-\pi + \sigma^+ + 2\pi$, and $2\pi + \sigma^+ - \pi$ (transitions (III) and (VI) in Fig. 2b).

The complete effective Hamiltonian is then

$$\mathcal{H}_{\text{eff}} = [\omega_S - \omega_{\text{mw}} - \omega_{\text{rf}} + \Delta(\alpha,0,0;\beta,1,1)]S_z + \omega(\alpha,0,0;\beta,1,1)S_x, \quad (40)$$

with the Bloch–Siegert shift [43] in first-order approximation

$$\Delta(\alpha,0,0;\beta,1,1) = 2\Delta(\alpha,0,0) = \frac{\omega_1^2}{2\omega_{\text{rf}}} + \frac{\omega_1^2}{2(2\omega_{\text{mw}}+\omega_{\text{rf}})} \approx \frac{\omega_1^2}{2\omega_{\text{rf}}} + \frac{\omega_1^2}{4\omega_{\text{mw}}} \quad (41)$$

and the effective field amplitude

$$\omega(\alpha,0,0;\beta,1,1) = -\frac{\omega_1\omega_2}{\omega_{\text{rf}}} + \frac{\omega_1\omega_2^3}{16(\omega_{\text{mw}}+\omega_{\text{rf}})\omega_{\text{rf}}^2} + \frac{\omega_1\omega_2^3}{8(\omega_{\text{mw}}-\omega_{\text{rf}})\omega_{\text{rf}}^2} + \frac{\omega_1^3\omega_2}{8\omega_{\text{mw}}(\omega_{\text{mw}}-\omega_{\text{rf}})\omega_{\text{rf}}} + \frac{\omega_1^3\omega_2}{16\omega_{\text{mw}}^2(2\omega_{\text{mw}}+\omega_{\text{rf}})} \approx -\frac{\omega_1\omega_2}{\omega_{\text{rf}}} + \frac{3\omega_1\omega_2^3}{16\omega_{\text{mw}}\omega_{\text{rf}}^2}. \quad (42)$$

Although the effective Hamiltonian in Eq. (40) correctly describes the change of the polarization during the two-photon transition, it fails to describe the behaviour of the coherences. Consequently, it also fails to describe the cw EPR signal, which is proportional to the steady-state coherences. The function subspace $\{|\alpha,0,0\rangle, |\beta,\ 1,1\rangle\}$ of $\mathcal{H}_{\text{eff}}$ implies that only coherences with frequency $\omega_{\text{mw}} + \omega_{\text{rf}}$ are present. But from Fig. 2b it becomes obvious that also coherences with frequencies of, for example, ω_{rf} and ω_{mw} exist, because levels with such spacings are involved in the transition.

The problem can be circumvented by going to a more sophisticated frame, in which only one coherence is present. This coherence should be a combination of the coherences of all important transition pathways in $\mathcal{H}_F$. As we have already seen in Section 2.1.3 the toggling frame is a convenient choice for the semiclassical description of a $\sigma^+ + k\times\pi$ transition. An analog approach will be used now for the quantized-field Hamiltonian.

Since for high photon numbers the quantized radiation field is equivalent to the classical field, we use the semiclassical Hamiltonian in Eq. (1) as starting point. This Hamiltonian is transformed to a singly rotating frame, rotating with ω_{mw}, and subsequently to the toggling frame

$$\begin{aligned}\mathcal{H}_{\text{TF},k} &= R(t)e^{i\omega_{\text{mw}}tS_z}\mathcal{H}_{\text{lab}}e^{-i\omega_{\text{mw}}tS_z}R^{-1}(t) - \omega_{\text{mw}}S_z - k\omega_{\text{rf}}S_z - 2\omega_2\cos(\omega_{\text{rf}}t)S_z \\ &= (\omega_S - \omega_{\text{mw}} - k\omega_{\text{rf}})S_z + R(t)e^{i\omega_{\text{mw}}tS_z}2\omega_1\cos(\omega_{\text{mw}}t)e^{-i\omega_{\text{mw}}tS_z}R^{-1}(t) \\ &= (\omega_S - \omega_{\text{mw}} - k\omega_{\text{rf}})S_z + \sum_{n=-\infty}^{+\infty} J_n\left(\frac{2\omega_2}{\omega_{\text{rf}}}\right)\omega_1 \\ &\quad\times\left[e^{i(k+n)\omega_{\text{rf}}tS_z}S_x e^{-i(k+n)\omega_{\text{rf}}tS_z} + e^{i(2\omega_{\text{mw}}+(k+n)\omega_{\text{rf}})tS_z}S_x e^{-i(2\omega_{\text{mw}}+(k+n)\omega_{\text{rf}})tS_z}\right], \end{aligned} \quad (43)$$

with $R(t)$ defined in Eq. (21). The parameter k of the toggling frame may be chosen arbitrarily and does not have to fulfill any kind of resonance condition, since the resonant transition will be selected later. To avoid complications we set $k = 0$.

The omission of the counter-rotating part does not significantly change the coupling between the levels. Fig. 2b indicates that absorption or emission of a σ^- mw photon is not involved. All transitions with more than one σ^+ mw photon (as for example (III) and (IV) in Fig. 2b) are much weaker than the concurring transitions,

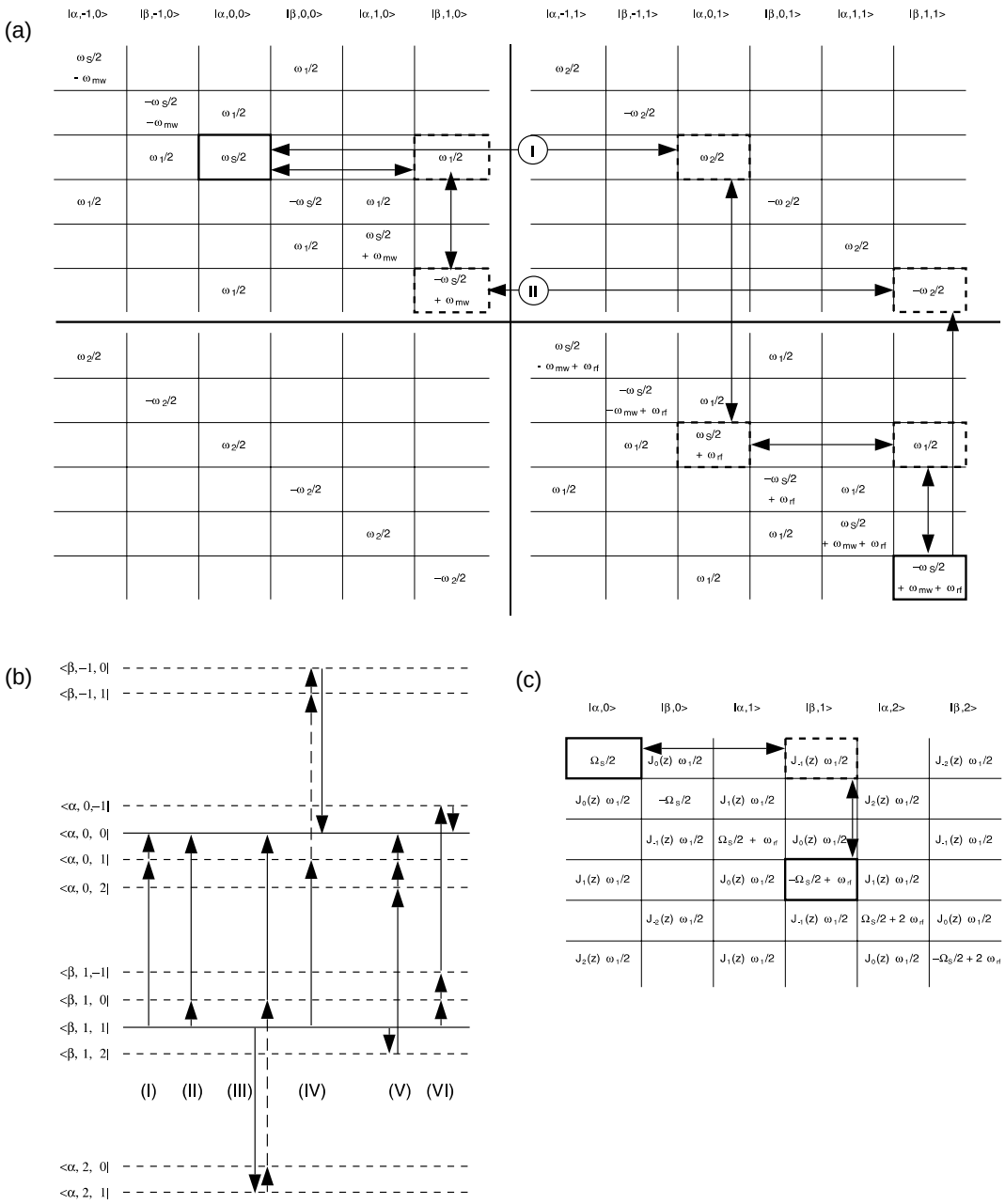

Fig. 2. (a) Segment of the two-mode Floquet space Hamiltonian $\mathcal{H}_{\mathrm{F}}$ in Eq. (33). The two degenerate levels $|\alpha,0,0\rangle$ and $|\beta,1,1\rangle$ are framed by full rectangles. The coupling elements and the intermediate levels of the two-photon transition are framed by dashed rectangles. The two pathways (I) and (II) are indicated by arrows. (b) Energy level scheme of the $(\omega_{\mathrm{S}}=\omega_{\mathrm{mw}}+\omega_{\mathrm{rf}})$ transition with the two contributing two-photon pathways (I) and (II) and the four four-photon pathways (III)-(VI). Black arrows: σ^{+}_{mw}, dashed arrows: σ^{-}_{mw}, grey arrows: π_{rf}. (c) Segment of the single-mode Floquet Hamiltonian $\mathcal{H}_{\mathrm{F,TF}}$ derived from Eq. (44).

because $\omega_1 \ll \omega_{\mathrm{mw}}$. The Bloch–Siegert shift on the other hand partially involves σ^- mw photons and will get lost without the counter-rotating part. We therefore have to reintroduce the Bloch–Siegert shift $\omega_1^2/(4\omega_{\mathrm{mw}})$ caused by the σ^- photons into the resonance offset. After omitting the counter-rotating term, the Hamiltonian $\mathcal{H}_{\mathrm{TF},0}$ is identical with the semiclassically derived Hamiltonian in Eq. (22) for $k=0$, apart from the Bloch–Siegert shift,

$$\mathcal{H}_{\mathrm{TF},0} = \left(\omega_{\mathrm{S}} - \omega_{\mathrm{mw}} + \frac{\omega_1^2}{4\omega_{\mathrm{mw}}}\right) S_z + \sum_{n=-\infty}^{+\infty} J_n\left(\frac{2\omega_2}{\omega_{\mathrm{rf}}}\right) \omega_1 \mathrm{e}^{\mathrm{i}n\omega_{\mathrm{rf}}tS_z} S_x \mathrm{e}^{-\mathrm{i}n\omega_{\mathrm{rf}}tS_z}. \tag{44}$$

From Eq. (44) the time-independent single-mode Floquet Hamiltonian $\mathcal{H}_{\mathrm{F,TF}}$ is constructed. A small segment is shown in matrix representation in Fig. 2c. In this

particular Floquet space the spin system is now considered as being dressed by one σ^+ mw photon and an arbitrary number of π rf photons.

$\mathcal{H}_{\mathrm{F,TF}}$ has a direct coupling element between two degenerate levels, taking into account all pathways where one σ^+ mw photon is absorbed. The coherence is described in the function space of $\mathcal{H}_{\mathrm{F,TF}}$. By transforming back to the singly rotating frame this single coherence is will be split up to a set of coherences corresponding to all involved virtual levels. The effective Hamiltonian of a resonant $\sigma^+ + k \times \pi$ multiple photon transition can now be calculated from $\mathcal{H}_{\mathrm{F,TF}}$ (see Fig. 2c) using Eqs. (36) and (39),

$$\mathcal{H}_{\mathrm{eff}} = \underbrace{\left[\Omega_{\mathrm{S}} - k\omega_{\mathrm{rf}} + \Delta(\alpha,0;\beta,k)\right]}_{\Delta_{1,k}} S_z + \underbrace{\left[J_{-k}\left(\frac{2\omega_2}{\omega_{\mathrm{rf}}}\right)\omega_1 + \omega(\alpha,0;\beta,k)\right]}_{\omega_{1,k}} S_x, \tag{45}$$

with the effective resonance offset $\Delta_{1,k}$ and the effective field amplitude $\omega_{1,k}$. The constant term $(1/2)k\omega_{\mathrm{rf}}\mathbf{1}$ has been omitted. For the resonance shift we get

$$\Delta(\alpha,0;\beta,k) \approx \frac{\omega_1^2}{4\omega_{\mathrm{mw}}} + \left(\frac{2\omega_1^2}{\omega_{\mathrm{rf}}}\right)\sum_{l\neq k}\frac{J_l^2\left(\frac{2\omega_2}{\omega_{\mathrm{rf}}}\right)}{(k-l)} \tag{46}$$

and for the higher-order contribution to the field amplitude we find

$$\omega(\alpha,0;\beta,k) \approx \left(\frac{\omega_1^3}{4\omega_{\mathrm{rf}}^2}\right)\sum_{l\neq k}\sum_{m\neq 0}\frac{J_{-l}\left(\frac{2\omega_2}{\omega_{\mathrm{rf}}}\right)J_{m-l}\left(\frac{2\omega_2}{\omega_{\mathrm{rf}}}\right)J_{m-k}\left(\frac{2\omega_2}{\omega_{\mathrm{rf}}}\right)}{(k-l)m}. \tag{47}$$

For $\omega_1 \ll \omega_{\mathrm{rf}}$ the second-order contributions $\Delta(\alpha,0;\beta,k)$ and $\omega(\alpha,0;\beta,k)$ may be neglected, and we obtain the formula

$$\mathcal{H}_{\mathrm{eff}} = (\Omega_{\mathrm{S}} - k\omega_{\mathrm{rf}})S_z + J_{-k}\left(\frac{2\omega_2}{\omega_{\mathrm{rf}}}\right)\omega_1 S_x. \tag{48}$$

This expression is equivalent to the Hamiltonian derived directly from the semiclassical toggling frame in Eq. (22) after omitting the time-dependent perturbations, with the difference that Eq. (48) is derived from a fully quantized Hamiltonian, thereby proving the absorption and emission of multiple photons.

For small arguments $z = 2\omega_2/\omega_{\mathrm{rf}} \ll 1$, the Bessel functions can alternatively be described as an ascending series with $n \in \mathbb{Z}_0$,

$$J_n(z) = \sum_{l=0}^{+\infty}\frac{(-1)^l\left(\frac{z}{2}\right)^{2l+n}}{l!\,(l+n)!}, \tag{49}$$

or simply by

$$J_n\left(\frac{2\omega_2}{\omega_{\mathrm{rf}}}\right) \approx \frac{1}{n!}\left(\frac{\omega_2}{\omega_{\mathrm{rf}}}\right)^n. \tag{50}$$

The effective transition amplitude is then given by

$$\omega_{1,k} \approx \omega_1\frac{[\mathrm{sign}(-k)]^k}{|k|!}\left(\frac{\omega_2}{\omega_{\mathrm{rf}}}\right)^{|k|}, \tag{51}$$

which is identical to Eqs. (10) and (14) derived with the semiclassical multiply tilted rotating-frame model.

2.2.4. Description of sidebands in cw EPR

The absorption cw EPR signal is proportional to the component of the steady-state density operator out-of-phase with the impinging mw. The steady-state solution can most easily be obtained in the frame of the effective Hamiltonian in Eq. (48) of the resonant transition, with the assumption that each $\sigma^+ + k \times \pi$ transition can be treated separately.

The density operator is transformed to the kth toggling frame by

$$\sigma_{\mathrm{TF},k}(t) = R(t)\sigma_{\mathrm{SRF}}(t)R^{-1}(t) = \sum_{n=-\infty}^{+\infty} J_n\left(\frac{2\omega_2}{\omega_{\mathrm{rf}}}\right)\mathrm{e}^{\mathrm{i}(k+n)\omega_{\mathrm{rf}}tS_z}\sigma_{\mathrm{TF}}(t)\mathrm{e}^{-\mathrm{i}(k+n)\omega_{\mathrm{rf}}tS_z}. \tag{52}$$

The density operator at thermal equilibrium, $\sigma_{\mathrm{SRF},0} = -S_z$, is not affected by this transformation, in contrast to the multiply tilted rotating-frame model. The steady-state solution for the density operator starting from thermal equilibrium is found to be

$$\sigma_{\mathrm{TF},k}^{\mathrm{ss}} = -\frac{\omega_{1,k}\Delta_{1,k}T_2^2}{1+\omega_{1,k}^2T_1T_2+\Delta_{1,k}^2T_2^2}S_x + \frac{\omega_{1,k}T_2}{1+\omega_{1,k}^2T_1T_2+\Delta_{1,k}^2T_2^2}S_y + \frac{1+\Delta_{1,k}^2T_2^2}{1+\omega_{1,k}^2T_1T_2+\Delta_{1,k}^2T_2^2}S_z, \tag{53}$$

with the effective resonance offset $\Delta_{1,k}$ and the effective field amplitude $\omega_{1,k}$ of the $\sigma^+ + k \times \pi$ transition. Neglecting the higher-order corrections in $\Delta_{1,k}$ and $\omega_{1,k}$ we find for the dispersion and absorption components

$$\{\sigma_{\mathrm{TF},k}^{\mathrm{ss}}\}_x = \frac{-(\Omega_{\mathrm{S}} - k\omega_{\mathrm{rf}})T_2^2\omega_1 J_{-k}\left(\frac{2\omega_2}{\omega_{\mathrm{rf}}}\right)}{1+\omega_1^2J_k^2\left(\frac{2\omega_2}{\omega_{\mathrm{rf}}}\right)T_1T_2+(\Omega_{\mathrm{S}}-k\omega_{\mathrm{rf}})^2T_2^2}, \tag{54}$$

$$\{\sigma_{\mathrm{TF},k}^{\mathrm{ss}}\}_y = \frac{T_2\,\omega_1 J_{-k}\left(\frac{2\omega_2}{\omega_{\mathrm{rf}}}\right)}{1+\omega_1^2J_k^2\left(\frac{2\omega_2}{\omega_{\mathrm{rf}}}\right)T_1T_2+(\Omega_{\mathrm{S}}-k\omega_{\mathrm{rf}})^2T_2^2}. \tag{55}$$

We remember that these transverse steady-state components are in the toggling frame of the respective sideband. However, the detection operator is given as $D = S_x$ in the singly rotating frame. The density operator

therefore has to be transformed back to the singly rotating frame,

$$\sigma_{\mathrm{SRF}}(t) = R^{-1}(t)\sigma_{\mathrm{TF}}(t)R(t) = \sum_{n=-\infty}^{+\infty} J_n\left(\frac{2\omega_2}{\omega_{\mathrm{rf}}}\right) \mathrm{e}^{-\mathrm{i}(k+n)\omega_{\mathrm{rf}}tS_z}\sigma_{\mathrm{TF}}(t)\mathrm{e}^{\mathrm{i}(k+n)\omega_{\mathrm{rf}}tS_z}. \tag{56}$$

A time-independent density operator in the toggling frame therefore leads to a series of terms in the singly rotating frame, oscillating with multiples of the modulation frequency. For the mw absorption signal we get

$$\{\sigma^{\mathrm{ss}}_{\mathrm{SRF}}\}_y = \sum_{n=-\infty}^{+\infty} \omega_1 J_n\left(\frac{2\omega_2}{\omega_{\mathrm{rf}}}\right) J_{-k}\left(\frac{2\omega_2}{\omega_{\mathrm{rf}}}\right) \times \frac{T_2\cos([k+n]\omega_{\mathrm{rf}}t) - (\Omega_{\mathrm{S}} - k\omega_{\mathrm{rf}})T_2^2\sin([k+n]\omega_{\mathrm{rf}}t)}{1+\omega_1^2 J_k^2\left(\frac{2\omega_2}{\omega_{\mathrm{rf}}}\right)T_1T_2 + (\Omega_{\mathrm{S}} - k\omega_{\mathrm{rf}})^2T_2^2}. \tag{57}$$

Summation over all possible multiple photon resonances results in the solution

$$\{\sigma^{\mathrm{ss}}_{\mathrm{SRF}}\}_y = \sum_{n=-\infty}^{+\infty}\sum_{k=-\infty}^{+\infty} \omega_1 J_n\left(\frac{2\omega_2}{\omega_{\mathrm{rf}}}\right) J_{-k}\left(\frac{2\omega_2}{\omega_{\mathrm{rf}}}\right) \times \frac{T_2\cos([k+n]\omega_{\mathrm{rf}}t) - (\Omega_{\mathrm{S}} - k\omega_{\mathrm{rf}})T_2^2\sin([k+n]\omega_{\mathrm{rf}}t)}{1+\omega_1^2 J_k^2\left(\frac{2\omega_2}{\omega_{\mathrm{rf}}}\right)T_1T_2 + (\Omega_{\mathrm{S}} - k\omega_{\mathrm{rf}})^2T_2^2}. \tag{58}$$

Apart from the neglected saturation parameter, Eq. (58) is identical to the classically derived expression [2] given in Eq. (7).

For a measured jth harmonic of the mw absorption signal only the terms of the density operator oscillating with $j\omega_{\mathrm{rf}}$ have to be taken into account. These terms are described by the relation $|k+n| = j$. The general expression for the jth harmonic absorption spectrum with $n = j-k$ and $n = -j-k$ is then

$$\{\sigma^{\mathrm{ss}}_{\mathrm{SRF}}\}_{y;j} = \sum_{k=-\infty}^{+\infty}\left[\frac{T_2\omega_1 J_{-k}\left(\frac{2\omega_2}{\omega_{\mathrm{rf}}}\right)\left[J_{j-k}\left(\frac{2\omega_2}{\omega_{\mathrm{rf}}}\right) + J_{-j-k}\left(\frac{2\omega_2}{\omega_{\mathrm{rf}}}\right)\right]}{1+\omega_1^2 J_k^2\left(\frac{2\omega_2}{\omega_{\mathrm{rf}}}\right)T_1T_2 + (\Omega_{\mathrm{S}} - k\omega_{\mathrm{rf}})^2T_2^2} \times\cos(\omega_{\mathrm{rf}}t) - \frac{(\Omega_{\mathrm{S}} - k\omega_{\mathrm{rf}})T_2^2\omega_1 J_{-k}\left(\frac{2\omega_2}{\omega_{\mathrm{rf}}}\right)\left[J_{j-k}\left(\frac{2\omega_2}{\omega_{\mathrm{rf}}}\right) - J_{-j-k}\left(\frac{2\omega_2}{\omega_{\mathrm{rf}}}\right)\right]}{1+\omega_1^2 J_k^2\left(\frac{2\omega_2}{\omega_{\mathrm{rf}}}\right)T_1T_2 + (\Omega_{\mathrm{S}} - k\omega_{\mathrm{rf}})^2T_2^2} \times\sin(\omega_{\mathrm{rf}}t)\right]. \tag{62}$$

Starting from Eq. (54) we also can calculate the dispersion spectrum

$$\{\sigma^{\mathrm{ss}}_{\mathrm{SRF}}\}_{x;j} = \sum_{k=-\infty}^{+\infty}\left[-\frac{(\Omega_{\mathrm{S}} - k\omega_{\mathrm{rf}})T_2^2\omega_1 J_{-k}\left(\frac{2\omega_2}{\omega_{\mathrm{rf}}}\right)\left[J_{j-k}\left(\frac{2\omega_2}{\omega_{\mathrm{rf}}}\right) + J_{-j-k}\left(\frac{2\omega_2}{\omega_{\mathrm{rf}}}\right)\right]}{1+\omega_1^2 J_k^2\left(\frac{2\omega_2}{\omega_{\mathrm{rf}}}\right)T_1T_2 + (\Omega_{\mathrm{S}} - k\omega_{\mathrm{rf}})^2T_2^2} \times\cos(j\omega_{\mathrm{rf}}t) - \frac{+T_2\omega_1 J_{-k}\left(\frac{2\omega_2}{\omega_{\mathrm{rf}}}\right)\left[J_{j-k}\left(\frac{2\omega_2}{\omega_{\mathrm{rf}}}\right) - J_{-j-k}\left(\frac{2\omega_2}{\omega_{\mathrm{rf}}}\right)\right]}{1+\omega_1^2 J_k^2\left(\frac{2\omega_2}{\omega_{\mathrm{rf}}}\right)T_1T_2 + (\Omega_{\mathrm{S}} - k\omega_{\mathrm{rf}})^2T_2^2}\sin(j\omega_{\mathrm{rf}}t)\right]. \tag{60}$$

For the *zeroth-harmonic absorption spectrum* (the spectrum obtained when the dc current is measured), only the constant term ($j = 0$) is of relevance, given by the relation $n = -k$. The complete zeroth-harmonic absorption spectrum is then

$$\{\sigma^{\mathrm{ss}}_{\mathrm{SRF}}\}_{y;j=0} = \sum_{k=-\infty}^{+\infty}\frac{T_2\omega_1 J_k^2\left(\frac{2\omega_2}{\omega_{\mathrm{rf}}}\right)}{1+\omega_1^2 J_k^2\left(\frac{2\omega_2}{\omega_{\mathrm{rf}}}\right)T_1T_2 + (\Omega_{\mathrm{S}} - k\omega_{\mathrm{rf}})^2T_2^2}. \tag{61}$$

The *first-harmonic absorption spectrum* ($j = 1$), which is usually measured in cw EPR, is obtained for $n = \pm 1 - k$,

$$\{\sigma^{\mathrm{ss}}_{\mathrm{SRF}}\}_{y;j=1} = \sum_{k=-\infty}^{+\infty}\left[\frac{T_2\omega_1 J_{-k}\left(\frac{2\omega_2}{\omega_{\mathrm{rf}}}\right)\left[J_{1-k}\left(\frac{2\omega_2}{\omega_{\mathrm{rf}}}\right) + J_{-1-k}\left(\frac{2\omega_2}{\omega_{\mathrm{rf}}}\right)\right]}{1+\omega_1^2 J_k^2\left(\frac{2\omega_2}{\omega_{\mathrm{rf}}}\right)T_1T_2 + (\Omega_{\mathrm{S}} - k\omega_{\mathrm{rf}})^2T_2^2} \times\cos(\omega_{\mathrm{rf}}t) - \frac{(\Omega_{\mathrm{S}} - k\omega_{\mathrm{rf}})T_2^2\omega_1 J_{-k}\left(\frac{2\omega_2}{\omega_{\mathrm{rf}}}\right)\left[J_{1-k}\left(\frac{2\omega_2}{\omega_{\mathrm{rf}}}\right) - J_{-1-k}\left(\frac{2\omega_2}{\omega_{\mathrm{rf}}}\right)\right]}{1+\omega_1^2 J_k^2\left(\frac{2\omega_2}{\omega_{\mathrm{rf}}}\right)T_1T_2 + (\Omega_{\mathrm{S}} - k\omega_{\mathrm{rf}})^2T_2^2} \times\sin(\omega_{\mathrm{rf}}t)\right]. \tag{62}$$

The meaning of these equations becomes clearer from the plot in Fig. 3, showing the field-swept spectra of the zeroth-harmonic signal and the in-phase and out-of-phase components of the first- and second-harmonic signal. Six multiple photon transitions are shown, centered around the single-photon transition; saturation is neglected. The zeroth-harmonic spectrum (Fig. 3b) consists of a center line and an infinite number of field-domain sidebands, with spacings $\Delta B = \omega_{\mathrm{rf}}/\gamma_e$. All lines have absorptive shape, with the intensity of the kth sideband proportional to $J_k^2(2\omega_2/\omega_{\mathrm{rf}})$.

The first-harmonic spectrum consists of the in-phase component with absorptive lineshape (Fig. 3c) and the out-of-phase component with dispersive lineshape (Fig. 3d). The spectra are anti-symmetric with respect to the center line. The second-harmonic spectra in Figs. 3e and f are again symmetric.

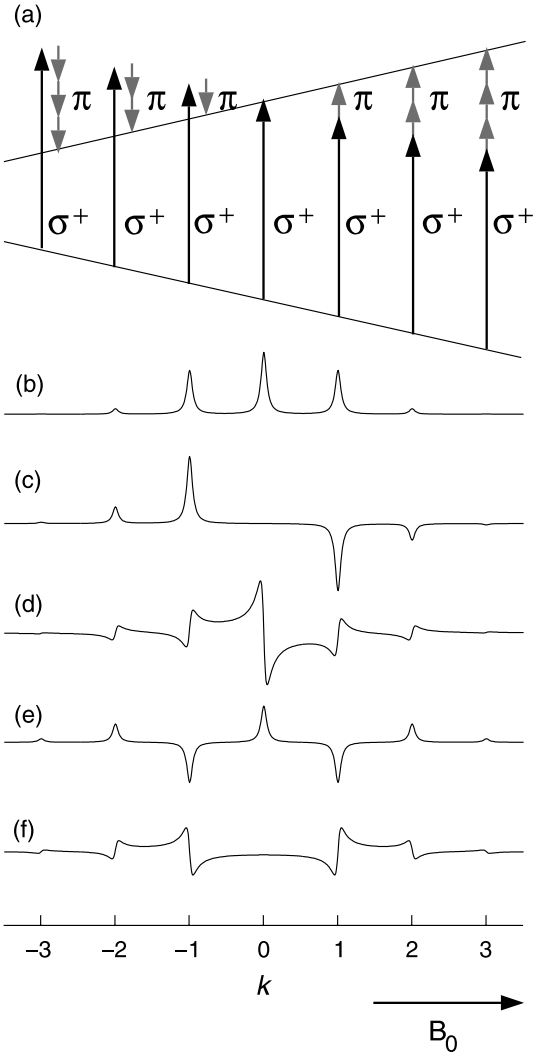

Fig. 3. Simulated field-swept cw EPR spectra of different harmonics of the modulation frequency, according to Eq. (59). The values k indicate the numbers of absorbed rf π photons: (a) multiple photon transitions; (b) zeroth-harmonic spectrum, $j = 0$; (c) first-harmonic spectrum, $j = 1$, in-phase with the rf; (d) corresponding out-of-phase spectrum; (e) second-harmonic spectrum, $j = 2$, in-phase with the rf; (f) corresponding out-of-phase spectrum.

2.2.5. Experimentally observed lineshape caused by overlapping sidebands

The first-harmonic signal in phase with the modulation frequency is the one usually measured in cw EPR, and in fact Eq. (62) can be converted to the commonly observed derivative lineshape. Below we show that this particular lineshape is formed by a large number of overlapping sidebands, or more exactly by pairs of interfering multiple photon resonances.

Neglecting saturation, the first-harmonic in-phase spectrum is

$$\{\sigma^{\mathrm{ss}}_{\mathrm{SRF}}\}_y = \sum_{k=-\infty}^{+\infty} J_{-k}\left(\frac{2\omega_2}{\omega_{\mathrm{rf}}}\right)\left[J_{1-k}\left(\frac{2\omega_2}{\omega_{\mathrm{rf}}}\right) + J_{-1-k}\left(\frac{2\omega_2}{\omega_{\mathrm{rf}}}\right)\right]\left(\frac{T_2\,\omega_1}{1+(\Omega_{\mathrm{S}}-k\omega_{\mathrm{rf}})^2\,T_2^2}\right). \tag{63}$$

With the recurrence relation [32] $J_{\nu-1}(z) + J_{\nu+1}(z) = (2\nu/z)J_\nu(z)$ we arrive at

$$\{\sigma^{\mathrm{ss}}_{\mathrm{SRF}}\}_y = \sum_{k=-\infty}^{+\infty} \frac{-k\,\omega_{\mathrm{rf}}}{\omega_2} J_k^2\left(\frac{2\omega_2}{\omega_{\mathrm{rf}}}\right)\left(\frac{T_2\,\omega_1}{1+(\Omega_{\mathrm{S}}-k\omega_{\mathrm{rf}})^2\,T_2^2}\right). \tag{64}$$

Terms with the same value of $|k|$ are combined, resulting in

$$\{\sigma^{\mathrm{ss}}_{\mathrm{SRF}}\}_y = \sum_{k=1}^{+\infty} \frac{-k\,\omega_{\mathrm{rf}}}{\omega_2} J_k^2\left(\frac{2\omega_2}{\omega_{\mathrm{rf}}}\right) \times \left[\frac{T_2\,\omega_1}{1+(\Omega_{\mathrm{S}}-k\omega_{\mathrm{rf}})^2\,T_2^2} - \frac{T_2\,\omega_1}{1+(\Omega_{\mathrm{S}}+k\omega_{\mathrm{rf}})^2\,T_2^2}\right]. \tag{65}$$

The term in the squared brackets can be replaced by

$$(-2k\,\omega_{\mathrm{rf}})K\,\frac{\mathrm{d}}{\mathrm{d}\Omega_{\mathrm{S}}}\left(\frac{T_2\,\omega_1}{1+\Omega_{\mathrm{S}}^2\,T_2^2}\right), \tag{66}$$

with the correction factor

$$K = \frac{\left(1+\Omega_{\mathrm{S}}^2\,T_2^2\right)^2}{\left(1+k^2\,\omega_{\mathrm{rf}}^2\,T_2^2\right)^2 + 2\,\Omega_{\mathrm{S}}^2\,T_2^2(1-k^2\,\omega_{\mathrm{rf}}^2\,T_2^2) + \Omega_{\mathrm{S}}^4\,T_2^4}. \tag{67}$$

The signal is then given by

$$\{\sigma^{\mathrm{ss}}_{\mathrm{SRF}}\}_y = \sum_{k=1}^{\infty} \frac{2\omega_{\mathrm{rf}}^2}{\omega_2} k^2 J_k^2\left(\frac{2\omega_2}{\omega_{\mathrm{rf}}}\right) K\,\frac{\mathrm{d}}{\mathrm{d}\Omega_{\mathrm{S}}}\left(\frac{T_2\,\omega_1}{1+\Omega_{\mathrm{S}}^2\,T_2^2}\right). \tag{68}$$

Since $K \approx 1$ for $k\,\omega_{\mathrm{rf}} \ll 1/T_2$, an upper bound $k_{\max}$ has to be found above which the terms of the sum can be neglected. A plot of the expression $k^2 J_k^2(z)$ (Fig. 4) shows an oscillatory behaviour for $k < z$ and a monotonic decay for $k > z$. We can therefore set $k_{\max} \approx z$, which leads to $k_{\max}\omega_{\mathrm{rf}} = 2\omega_2$.

For $2\omega_2 \ll 1/T_2$, K in Eq. (68) can be set to 1, and using the infinite sum [44]

$$\sum_{k=1}^{k_{\max}} k^2 J_k^2(z) \approx \sum_{k=1}^{\infty} k^2 J_k^2(z) = \left(\frac{z}{2}\right)^2 \tag{69}$$

we get for Eq. (68)

$$\{\sigma^{\mathrm{ss}}_{\mathrm{SRF}}\}_y \approx 2\omega_2\,\frac{\mathrm{d}}{\mathrm{d}\Omega_{\mathrm{S}}}\left(\frac{T_2\,\omega_1}{1+\Omega_{\mathrm{S}}^2\,T_2^2}\right). \tag{70}$$

Eq. (70) describes the derivative lineshape commonly observed in cw EPR. The amplitude is proportional to

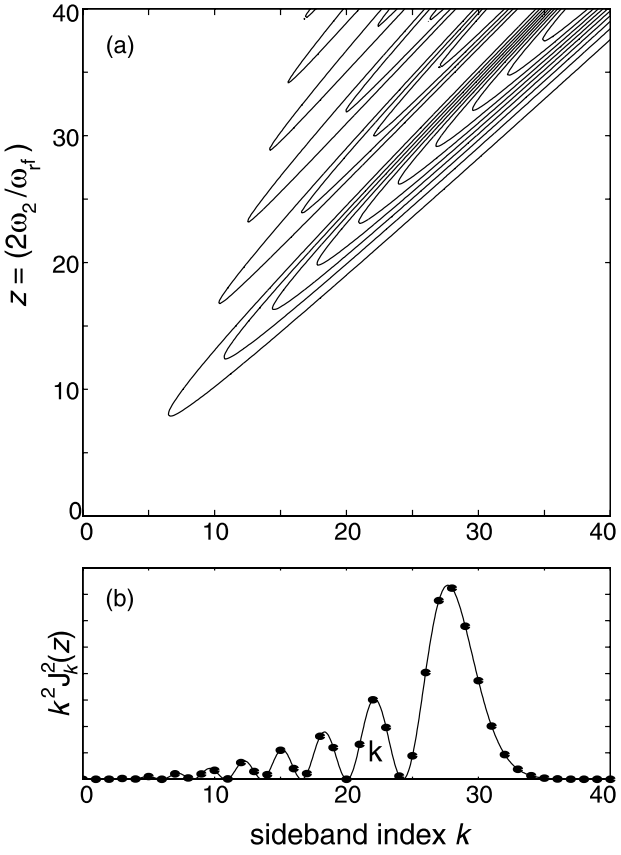

Fig. 4. (a) Contour plot of the expression $k^2 J_k^2(z)$ as a function of the sideband index k and the rf parameter $z = 2\omega_2/\omega_{rf}$. (b) Plot of $k^2 J_k^2(z)$ for an rf parameter $z = (2\omega_2/\omega_{rf}) = 30$. The contributions of the $\sigma^+ \pm k \times \pi$ multiple photon transitions to the first-harmonic cw EPR signal are shown as black dots.

the modulation amplitude and does not depend on the modulation frequency. It also reproduces the experimental condition for an undistorted signal, namely that the modulation amplitude $2\omega_2$ has to be much smaller than the homogeneous linewidth. If the modulation amplitude is much larger than the homogeneous linewidth, the lineshape consists of unresolved sidebands with reversed signs and a spacing ΔB approximately twice the amplitude of the linearly polarized rf field. This corresponds to the effect normally exploited to calibrate the modulation amplitude of cw EPR spectrometers.

The expression can be extended to the more general case of an inhomogeneously broadened line, which consists of a statistical distribution of unresolved homogeneously broadened lines. When the modulation frequency is larger than the homogeneous linewidth, the sidebands are resolved. Nevertheless the convolution of the sideband pattern with the statistical distribution pattern will also result in the derivative lineshape of the inhomogeneously broadened line, as long as the modulation amplitude does not exceed the inhomogeneous linewidth.

It is rather astonishing that the cw EPR derivative signal consists of a large number of multiple photon transitions, with the signal formed mainly by transitions involving the absorption of one mw photon and the absorption and emission of approximately $(2\omega_2/\omega_{rf})$ rf photons. In a standard cw EPR experiment, for example, with $\omega_{rf}/2\pi = 100\,\text{kHz}$ and a modulation amplitude of 0.1 mT ($2\omega_2/2\pi \approx 3\,\text{MHz}$), the two multiple photon transitions with the largest contribution to the signal are $\sigma^+ \pm 28 \times \pi$.

2.3. Relation between field modulation and frequency modulation

An often discussed question in cw EPR spectroscopy is the equivalence of field modulation and frequency modulation. In the latter case the frequency of the mw is modulated instead of the static field. The signal is obtained by phase sensitive detection with the modulation frequency as reference. Statements about the equivalence of the two techniques are contradictory [45–47]. Applying the formalisms used in this work the principal difference between the two techniques can easily be explained and understood.

The Hamiltonian for frequency-modulation cw EPR is given by

$$\mathcal{H}_{\text{lab}} = \omega_S S_z + 2\omega_1 \cos\left[\omega_{mw} t + \left(\frac{\omega_3}{\omega_m}\right)\sin(\omega_m t)\right] S_x, \tag{71}$$

with the modulation amplitude ω_3 and the modulation frequency ω_m. The time-dependent mw frequency is then given by the derivative of the argument of the cosine, $\omega_{mw}(t) = \omega_{mw} + \omega_3 \cos(\omega_m t)$. The cosine is split in the two circularly polarized components. After transformation to a frame rotating with ω_{mw} and omitting of the counter-rotating terms we get

$$\begin{aligned}\mathcal{H}_{\text{SRF}} &= (\omega_S - \omega_{mw}) S_z \\ &\quad + e^{-i\left(\frac{\omega_3}{\omega_m}\right)\sin(\omega_m t) S_z} \omega_1 S_x e^{i\left(\frac{\omega_3}{\omega_m}\right)\sin(\omega_m t) S_z} \\ &= \Omega_S S_z + \sum_{n=-\infty}^{+\infty} J_n\left(\frac{\omega_3}{\omega_m}\right)\omega_1 e^{-in\omega_m t S_z} S_x e^{in\omega_m t S_z},\end{aligned} \tag{72}$$

which looks similar to Eq. (44). The mw band is split in frequency sidebands with intensities $J_n(\omega_3/\omega_m)\omega_1$. The signal is proportional to the transverse magnetization out-of-phase to the mw center band, since the unmodulated mw frequency is used as reference for detection. If further transformations are applied, the obtained steady-state density operator has to be transformed back to this singly rotating frame to calculate the steady-state signal.

An argument used to explain the equivalency of field and frequency modulation is the similarity of the Bloch equations, which as a consequence leads to equivalent steady-state solutions. To reach a frame where the frequency-modulation Hamiltonian in Eq. (71) is equivalent to the field-modulation Hamiltonian in the singly

rotating frame [Eq. (2)], Eq. (71) has to be transformed to a toggling frame with $k = 0$, in analogy to Eq. (22),

$$\begin{aligned}\mathcal{H}_{\mathrm{TF},0} &= \mathrm{e}^{\mathrm{i}\left(\frac{\omega_3}{\omega_m}\right)\sin(\omega_m t)S_z}\mathcal{H}_{\mathrm{SRF}}\mathrm{e}^{-\mathrm{i}\left(\frac{\omega_3}{\omega_m}\right)\sin(\omega_m t)S_z} \\ &\quad - \omega_3\cos(\omega_m t)S_z \\ &= \Omega_{\mathrm{S}}S_z + \omega_1 S_x - \omega_3\cos(\omega_m t)S_z. \end{aligned} \tag{73}$$

Eq. (73) is now in fact equivalent to Eq. (2), with $2\omega_2 = -\omega_3$, and the steady-state solution will lead to the same results as for field modulation. But as mentioned above the toggling frame is not the suitable frame to describe detection.

If alternatively Eq. (72) is transformed to a doubly rotating frame rotating with $k\omega_m$ the resonant transition of the kth mw frequency sideband is given by

$$\begin{aligned}\mathcal{H}_{\mathrm{DRF},k} &= (\omega_{\mathrm{S}} - \omega_{\mathrm{mw}} - k\omega_m)S_z \\ &\quad + \sum_{n=-\infty}^{+\infty} J_n\left(\frac{\omega_3}{\omega_m}\right)\omega_1\mathrm{e}^{\mathrm{i}(k-n)\omega_m t S_z}S_x\mathrm{e}^{-\mathrm{i}(k-n)\omega_m t S_z} \\ &\approx (\Omega_{\mathrm{S}} - k\omega_m)S_z + J_{-k}\left(\frac{\omega_3}{\omega_m}\right)\omega_1 S_x. \end{aligned} \tag{74}$$

The steady-state solution of the density operator has to be transformed back to the singly rotating frame, $\sigma^{\mathrm{ss}}_{\mathrm{SRF}} = \exp(-\mathrm{i}k\omega_m t S_z)\sigma^{\mathrm{ss}}_{\mathrm{DRF},k}\exp(\mathrm{i}k\omega_m t S_z)$. Summing over all possible resonances, in analogy to Eq. (58), gives then the signal

$$\begin{aligned}\{\sigma^{\mathrm{ss}}_{\mathrm{SRF}}\}_y &= \sum_{k=-\infty}^{+\infty}\omega_1 J_{-k}\left(\frac{\omega_3}{\omega_{\mathrm{rf}}}\right) \\ &\quad \times \frac{T_2\cos(k\omega_{\mathrm{rf}}t) - (\Omega_{\mathrm{S}} - k\omega_{\mathrm{rf}})T_2^2\sin(k\omega_{\mathrm{rf}}t)}{1 + \omega_1^2 J_k^2\left(\frac{2\omega_2}{\omega_{\mathrm{rf}}}\right)T_1T_2 + (\Omega_{\mathrm{S}} - k\omega_{\mathrm{rf}})^2T_2^2}. \end{aligned} \tag{75}$$

This result differs from the expression derived for field modulation in Eq. (58). Since in first approximation only single-photon processes take place, every sideband transition produces only coherence between the two resonant levels. A jth harmonic thus consists only of two sidebands with $|k| = j$.

The results prove that the field-modulation and the frequency-modulation technique are not equivalent, neither in their mathematical formulation (Eq. (58) vs. Eq. (75)) nor physically ($\sigma^+ + k \times \pi$ multiple photon transitions vs. single σ^+ photon transition).

3. Experiment

3.1. Sample

Lithium phthalocyanine (LiPc) was used as an $S = 1/2$ model system. LiPc is synthesized by electrochemical oxidation of Li_2Pc [48] and has a very narrow line with values as small as $\Delta B_{\mathrm{pp}} = 1\,\mu\mathrm{T}$ [49]. The g-value is $g = 2.0020$, with an anisotropy too small to be resolved [50]. The measured linewidths of $\Gamma_{\mathrm{FWHH}} = 4$–$8\,\mu\mathrm{T}$ allowed us to resolve sidebands for modulation frequencies in the range of a few megacycles.

In our theoretical description relaxation is treated phenomenologically. The relaxation, in the case of LiPc exchange narrowing due to fast spin exchange, is assumed to have no influence on the multiple photon resonance phenomena.

A microcrystal ($0.3 \times 0.1 \times 0.1\,\mathrm{mm}^3$) of LiPc (LETI, Grenoble, France) was used. The single crystal was fixed in a Q-band quartz tube (1.6 mm outer diameter) by glass wool. The tube was evacuated and sealed. For the X-band experiments the Q-band sample was put into an X-band quartz tube (3.8 mm outer diameter).

3.2. Spectrometer

3.2.1. X-band spectrometer

A commercial X-band pulse EPR spectrometer (Bruker Elexsys E580) was used. The rf modulation field parallel to the static magnetic field was produced by the ENDOR coil of a pulse ENDOR probehead (Bruker ER 4118X-MD5-EN) rotated by 90° around its axis. The rf was amplified by a broad-band amplifier (Amplifier Research, model 250A250A).

Since the preamplifier of the mw bridge (Bruker ESP 380-1010) is designed for a modulation frequency of 100 kHz, the signal from the diode of the cw channel was used without prior amplification. For this purpose the signal after the diode was split into two parts by a T-splitter. One part was connected to the internal preamplifier to allow tuning and automatic frequency control (77 kHz). The other part was used as the input signal for the PSD, with 1-MΩ input resistance. The cavity was tuned and critically coupled as in a standard cw EPR experiment.

3.2.2. Q-band spectrometer

A home-built Q-band spectrometer [51] equipped with a Bruker Elexsys E580 console, a DICE ENDOR unit, a PatternJet pulse sequence programmer and a SpecJet transient digitizer was used. A cw ENDOR probehead (Bruker ER5106-QTE) was rotated by 90°. The rf amplifier was a Kalmus 137C. The signal was again split and fed to the internal preamplifier and the external PSD.

3.2.3. Field sweep setup

The setup used for measuring the first and second harmonic of the signal as a function of B_0 (corresponding to a standard cw EPR experiment) was the same for both spectrometers (Fig. 5). The signal from the mw bridge was fed to an external PSD (Stanford

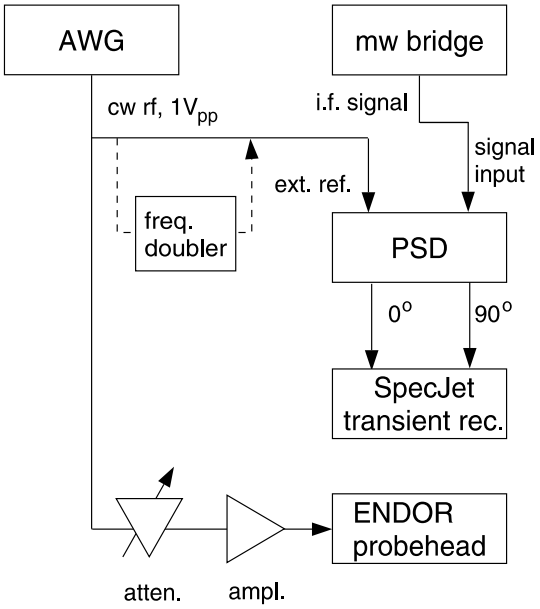

Fig. 5. Setup for the sideband field-sweep EPR experiment.

Research rf lock-in amplifier SR844). The modulation frequency was produced by an arbitrary waveform generator (LeCroy LW420B) and split by a power splitter. One part was used as external reference of the PSD, the other part was amplified and fed to the ENDOR coil.

The PSD provides the signal in-phase and out-of-phase to the reference signal. The two signals were digitized and averaged by the SpecJet transient recorder of the Elexsys console. Phase correction was done either numerically or experimentally, by changing the phases of the two channels. The second-harmonic sideband signal was measured with the same setup. The reference frequency was obtained by feeding the original reference signal through a frequency doubler.

4. Experimental results

4.1. Dependence on the rf amplitude

Since the physical origin of sidebands in EPR has not been investigated in detail so far, spectra with well resolved sideband structure are rare in EPR literature. For cw NMR an exemplary water proton spectrum was reported [52]. In our experiments we measured spectra with modulation frequencies between 100 kHz and 20 MHz. While the lower limit was given by the used setup, the higher limit was given by the rapidly decreasing intensities of sidebands for increasing modulation frequencies.

EPR spectra measured at Q-band with a modulation frequency of 5 MHz (Fig. 6) show clearly resolved sidebands. Figs. 6a and b depict the in-phase and out-of-phase first-harmonic spectra, with absorptive and dis-

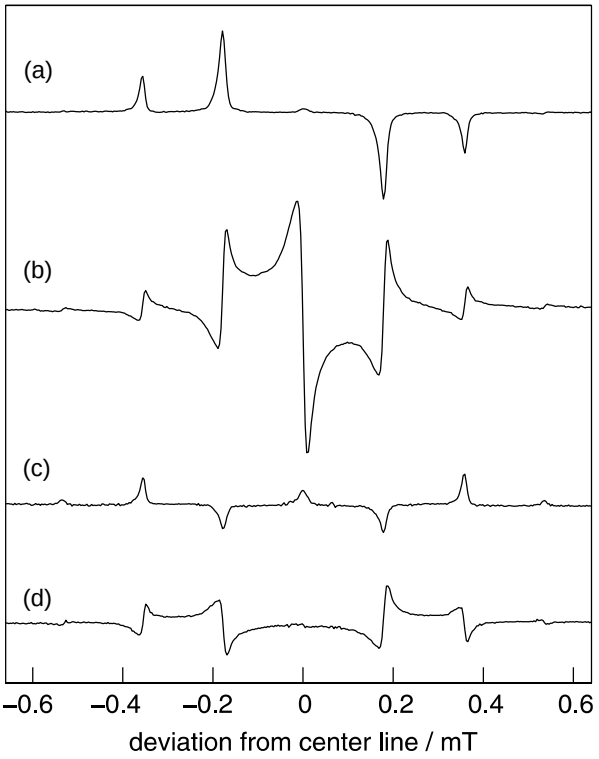

Fig. 6. EPR spectra of LiPc at Q-band, modulation frequency 5 MHz, mw power 2 mW: (a) first-harmonic spectrum, in-phase with the modulation frequency; (b) corresponding out-of-phase spectrum; (c) second-harmonic in-phase spectrum; (d) corresponding out-of-phase spectrum.

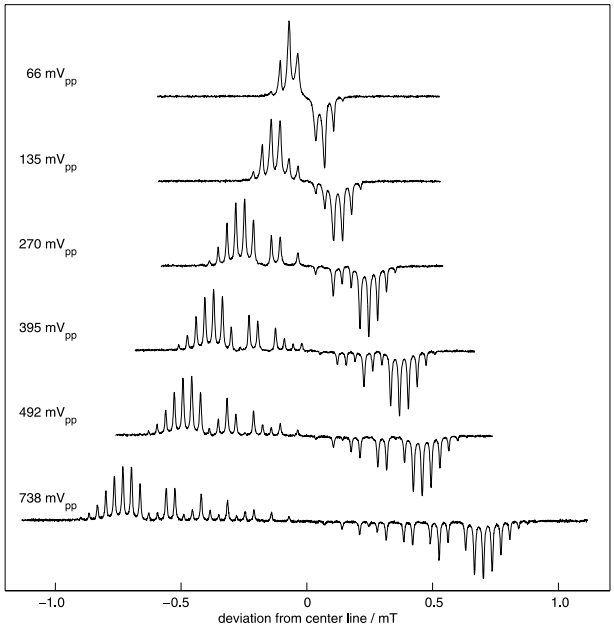

Fig. 7. Series of first-harmonic EPR spectra of LiPc recorded at X-band, in phase with the modulation frequency of 1 MHz. The modulation amplitude is given by the voltage measured over the 50-Ω termination of the ENDOR coil. Microwave power $P_{mw} = 0.6$ mW.

persive lineshapes, as predicted by theory (Eq. (62) and Figs. 3c and d). The second-harmonic spectra shown in Figs. 6c and d were measured by doubling the reference frequency. Again the spectra fit to the sideband patterns predicted in Figs. 3e and f.

For larger rf amplitudes a pattern of the sidebands with intensities similar to Fig. 4b is expected. The series of X-band EPR spectra with $\omega_{rf}/2\pi = 1$ MHz in Fig. 7 shows such patterns. The index of the sideband with maximum intensity is approximately linearly dependent on the rf amplitude, as expected from Fig. 4a.

The enlarged high-field part of the 738 mV_{pp} spectrum in Fig. 8a shows 25 resolved sidebands. Thus, the absorption and emission of up to 25π rf photons can be observed in this experiment. The sideband with maximum intensity has index $k_{max} = 20$. A simulation of this pattern based on Eq. (64) is in good agreement with the measurements. To get higher accuracy the saturation term

$$S = \sum_{k=-\infty}^{+\infty} \frac{-k\,\omega_{rf}}{\omega_2} J_k^2\left(\frac{2\omega_2}{\omega_{rf}}\right) \times \left(\frac{T_2\,\omega_1}{1+\omega_1^2 J_k^2\left(\frac{2\omega_2}{\omega_{rf}}\right) T_1 T_2 + (\Omega_S - k\omega_{rf})^2 T_2^2}\right) \quad (76)$$

has to be reintroduced in Eq. (64). The amplitude I_k of the kth sideband is then proportional to

$$I_k \propto \left(\frac{k J_k^2\left(\frac{2\omega_2}{\omega_{rf}}\right)}{1+\omega_1^2 J_k^2\left(\frac{2\omega_2}{\omega_{rf}}\right) T_1 T_2}\right). \quad (77)$$

The bar plot based on this equation is given in Fig. 8b and reproduces the spectrum in Fig. 8a very well. The relative intensities of the sidebands are extremely sensitive to changes of $(2\omega_2/\omega_{rf})$ and allow thus for an accurate determination of the rf amplitude. In the given example we find $2\omega_2/2\pi = 22.04$ MHz. The influence of the saturation parameter $\omega_1^2 T_1 T_2$ is less pronounced and consequently the estimated value $\omega_1^2 T_1 T_2 \approx 40$ less exact. Although the found saturation term is very large, the sidebands are not strongly saturated. This is because the *effective* saturation parameter $\omega_1^2 J_k^2(2\omega_2/\omega_{rf}) T_1 T_2$ is still small.

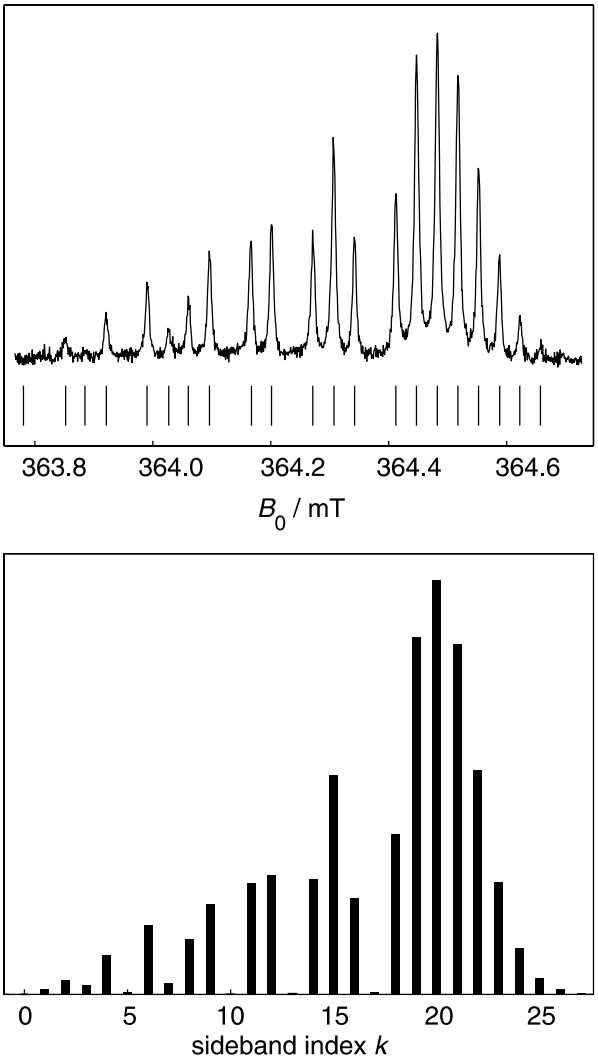

Fig. 8. Sideband pattern in the first-harmonic EPR spectrum. (a) Spectrum of LiPc recorded at X-band (high-field branch, multiplied by a factor -1), in phase with the modulation frequency of 1 MHz, rf amplitude 738 mV_{pp}. The positions of the sidebands are labelled. The most left label indicates the position of the center line. The sideband with maximum intensity has index $k = 20$. (b) Bar plot of Eq. (77), describing the intensity of the sidebands in the first-harmonic spectrum, $(2\omega_2/\omega_{rf}) = 22.04$, $\omega_1^2 T_1 T_2 = 40$.

4.2. Dependence on the mw amplitude, saturation broadening

According to Eq. (77) the saturation broadening depends on the sideband index k. This is experimentally verified in Fig. 9, where the mw power is increased in steps of 10 dB. The intensities of the two upmost spectra are not proportional to $\sqrt{10}$, indicating that the lines start to saturate. At higher mw power the sidebands with larger intensity (larger effective transition amplitude) broaden more than the sidebands with weaker intensity. In the spectrum with maximum mw power most of the lines are no longer resolved. Only the sidebands with the weakest effective transition amplitude remain unsaturated. From the experimental data it can be concluded that Eq. (59) is valid and describes the cw EPR signal accurately.

4.3. Phenomenological lineshape, unresolved sideband structure

As implied in Section 2.2.5 the derivative lineshape observed in cw EPR, as well as the distorted lineshape observed for modulation amplitudes larger than a certain fraction of the linewidth, are caused by pairs of interfering multiple photon transitions with absorptive

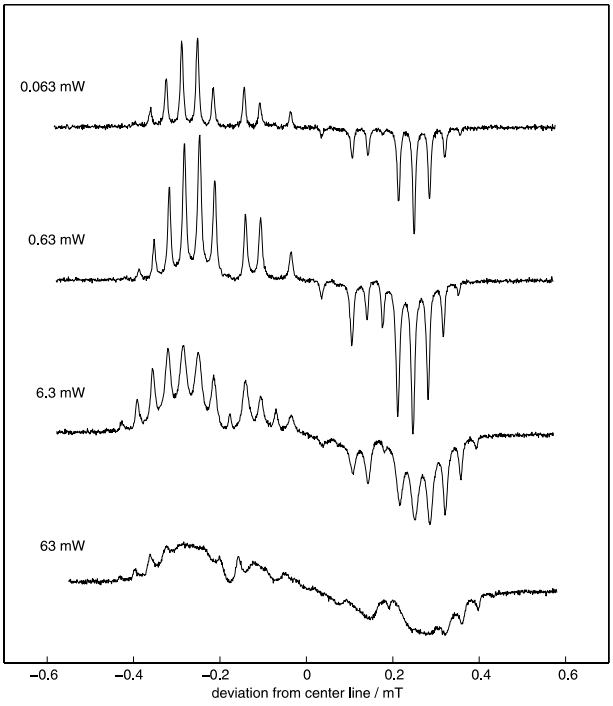

Fig. 9. Series of first-harmonic EPR spectra of LiPc recorded at X-band for different incident mw powers, in phase with the modulation frequency of 1 MHz.

lineshape. This astonishing finding is experimentally verified, in Fig. 10, which shows two series of spectra, measured with different rf amplitudes. The spectra in Fig. 10a, obtained with a modulation frequency of 500 kHz, show sideband pattern that are still resolved. The splitting between the two most intense sidebands are linearly dependent on the modulation amplitude, as already observed in Fig. 7. Although the different sidebands are still distinguishable, it is already visible that for weak modulation amplitudes the spectrum resembles a derivative lineshape, whereas for strong modulation it consists of two groups of peaks known from overmodulated cw EPR spectra. The out-of-phase signal is averaged to zero. When the modulation frequency is further reduced to 100 kHz (Fig. 10b), the sidebands are no longer resolved. We now have reached the standard cw EPR experiment.

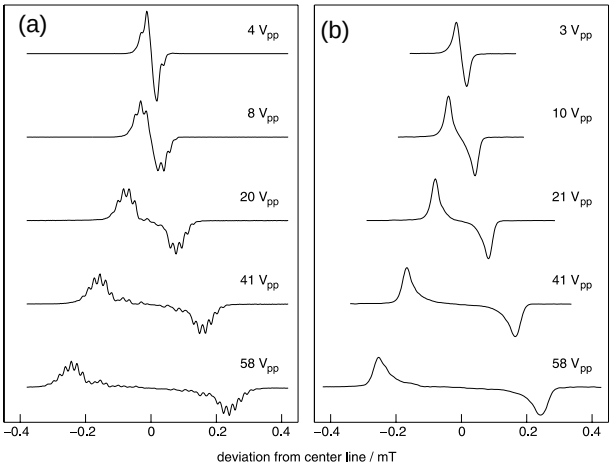

Fig. 10. EPR spectra of LiPc recorded at Q-band for different modulation amplitudes, labelled by the voltage measured over the 50-Ω termination of the ENDOR coil. (a) Modulation frequency 500 kHz, the sideband structure is still resolved. (b) Modulation frequency 100 kHz, the sidebands are no longer resolved.

5. Conclusions

In this work, we showed theoretically and experimentally that sidebands in cw EPR spectra are actually multiple photon transitions. In these transitions one mw σ^+ photon is absorbed and an arbitrary number of rf π photons is absorbed or emitted. Furthermore, we demonstrated that the derivative shape of the EPR lines consists of unresolved sideband patterns of these lines. Thus, the first-harmonic in-phase EPR signal usually measured in a cw EPR experiment does not represent a single-photon transition, but is rather a superposition of a large number of multiple photon transitions. The single-photon transition does not even contribute to the observed cw EPR signal.

We described the process of a multiple photon transition semiclassically in a toggling frame, which was found to be more convenient for the description of $\sigma^+ + k \times \pi$ transitions than the tilted rotating-frame approach. It is not restricted to weak mw and rf amplitudes, and also describes the higher harmonics of the modulation frequency in the cw EPR signal. The existence of the multiple photon transitions was proven by using the function space of a Hamiltonian including the quantized mw and rf radiation fields. Using the toggling frame approach an effective Hamiltonian for an arbitrary sideband transition was derived that included not only the two $\sigma^+ + k \times \pi$ transition pathways but also pathways with higher numbers of rf π photons. This effective frame is equivalent to the semiclassical Hamiltonian in the kth toggling frame.

By comparison with the analogous solutions for frequency-modulation EPR it was shown that the field-modulation and the frequency-modulation techniques are not equivalent.

Based on the effective Hamiltonians we derived an expression for the steady-state density operator in the singly rotating frame, which completely describes all sidebands in all modulation frequency harmonics of the cw EPR signal. The expression is identical with the solution obtained classically. In the first-harmonic spectrum the sidebands with maximum intensity were found to have the sideband index $k \approx \pm 2\omega_2/\omega_{rf}$. For linewidths larger than the modulation frequency the sidebands are not resolved. The calculated sideband pattern

was shown to merge into the lineshape commonly observed in cw EPR, with a derivative shape for modulation amplitudes smaller than the linewidth, and two lines with reversed signs and split by twice the modulation amplitude in case of strong overmodulation.

The experimental data fully verify the theoretical predictions about intensities and lineshapes. The relative intensities of the sidebands were found to depend in a very sensitive way on the actual rf amplitude. This can be exploited as a method to determine rf amplitudes in ENDOR experiments. The saturation of single sidebands was shown to depend strongly on the effective field amplitude of the multiple photon transition.

Although the finding that cw EPR derivative signals consists of multiple photon transitions has little effect on the daily work of an EPR spectroscopist, it could help to understand effects connected with the lineshape of transitions, as for example saturation broadening. It was shown that the single-photon transition, with transition amplitude $\omega_1 J_0(2\omega_2/\omega_{\mathrm{rf}})$, gives no contribution to the cw EPR signal and the signal is mainly produced by a pair of interfering sidebands with an effective field amplitude of approximately

$$\omega_{1,k_{\max}} = \omega_1 J_{(2\omega_2/\omega_{\mathrm{rf}})}(2\omega_2/\omega_{\mathrm{rf}}) \approx \omega_1 \left[3^{2/3}\Gamma\left(\frac{2}{3}\right)\right]^{-1} (\omega_{\mathrm{rf}}/\omega_2)^{1/3}.$$

Consequently, the effective saturation of a line is much lower than the saturation of the single-photon transition observed without field modulation. The implications of this finding have to be further investigated.

The application of the multiple photon transition Hamiltonian is not restricted to cw EPR. It also gives new insights to experiments using bichromatic pulses [20,21] and to the non-linear behaviour of spin systems. Another possible application could be the development of frequency-swept techniques, where the frequency of the applied rf field is varied and not the magnetic field. Such methods would open new possibilities for further developments in cw EPR spectroscopy.

References

[1] F. Bloch, W.W. Hansen, M. Packard, Phys. Rev. 70 (1946) 474.
[2] O. Haworth, R.E. Richards, Prog. NMR Spectrosc. 1 (1966) 1.
[3] I. Miyagawa, Y. Hayashi, Y. Kotake, J. Magn. Reson. 25 (1977) 183.
[4] B. Rakvin, T. Islam, I. Miyagawa, Phys. Rev. Lett. 50 (1983) 1313.
[5] J.S. Hyde, P.B. Sczaniecki, W. Froncisz, J. Chem. Soc. Faraday Trans. I 85 (1989) 3901.
[6] P.B. Sczaniecki, J.S. Hyde, J. Chem. Phys. 94 (1991) 5907.
[7] H.S. Mchaourab, J.S. Hyde, J. Chem. Phys. 98 (1993) 1786.
[8] T.-S. Ho, S.-I. Chu, J. Phys. B 17 (1984) 2101.
[9] S.-I. Chu, Adv. Atom. Mol. Phys. 21 (1985) 197.
[10] M. Jeleń, W. Froncisz, J. Chem. Phys. 109 (1998) 9272.
[11] P. Bucci, P. Cavaliere, S. Santucci, J. Chem. Phys. 52 (1970) 4041.
[12] P. Bucci, M. Martinelli, S. Santucci, J. Chem. Phys. 53 (1970) 4524.
[13] Y. Zur, M.H. Levitt, S. Vega, J. Chem. Phys. 78 (1983) 5293.
[14] E.M. Krauss, S. Vega, Phys. Rev. A 34 (1986) 333.
[15] G. Goelman, D.B. Zax, S. Vega, J. Chem. Phys. 87 (1987) 31.
[16] R. Boscaino, F.M. Gelardi, G. Messina, Solid State Commun. 46 (1983) 747.
[17] R. Boscaino, F.M. Gelardi, G. Messina, Phys. Lett. A 97 (1983) 413.
[18] R. Boscaino, F.M. Gelardi, G. Messina, Phys. Rev. A 28 (1983) 495.
[19] B. Clerjaud, A. Gelineau, Phys. Rev. Lett. 48 (1982) 40.
[20] I. Gromov, A. Schweiger, J. Magn. Reson. 146 (2000) 110.
[21] M. Kälin, I. Gromov, A. Schweiger, Multiphoton resonances in pulse EPR, 14th ISMAR Conference Rhodes, 2001. Available from: http://e-collection.ethbib.ethz.ch/show?type=inkonf&nr=11.
[22] J. Burget, M. Odehnal, V. Petříček, J. Šàcha, L. Trlifaj, Czech. J. Phys. B 11 (1961) 719.
[23] R. Boscaino, G. Messina, Physica C 138 (1986) 179.
[24] R. Karplus, Phys. Rev. 73 (1948) 1027.
[25] B. Smaller, Phys. Rev. 83 (1951) 812.
[26] K. Halbach, Helv. Phys. Acta 29 (1956) 37.
[27] H. Primas, Helv. Phys. Acta 31 (1958) 17.
[28] W.A. Anderson, NMR and EPR spectroscopy, Varian's 3rd Annual Workshop on NMR and EPR, Pergamon Press, Oxford, 1960, p. 180.
[29] J.D. Macomber, J.S. Waugh, Phys. Rev. 140 (1965) A1494.
[30] F. Bloch, Phys. Rev. 70 (1946) 460.
[31] R.R. Ernst, G. Bodenhausen, A. Wokaun, Principles of Nuclear Magnetic Resonance in One and Two Dimensions, Oxford University Press, Oxford, UK, 1997.
[32] M. Abramowitz, I.A. Stegun (Eds.), Handbook of Mathematical Functions, Dover, New York, 1968.
[33] C. Cohen-Tannoudji, J. Dupont-Roc, G. Grynberg, Atom–Photon Interactions, Wiley, New York, 1992.
[34] R.J. Glauber, Phys. Rev. 131 (1963) 2766.
[35] N. Polonsky, C. Cohen-Tannoudji, J. Phys. 26 (1965) 409.
[36] C. Cohen-Tannoudji, in: Cargèse Lectures in Physics, vol. 2, Gordon and Beach, New York, 1968, p. 347.
[37] M. Giordano, D. Leporini, M. Martinelli, L. Pardi, S. Santucci, C. Umeton, Phys. Rev. A 38 (1988) 1931.
[38] J.H. Shirley, Phys. Rev. 138 (1965) B979.
[39] S. Vega, Encyclopedia of Nuclear Magnetic Resonance, Wiley, Chichester, UK, 1996.
[40] T.O. Levante, M. Baldus, B.H. Meier, R.R. Ernst, Mol. Phys. 86 (1995) 1195.
[41] M. Kälin, A. Schweiger, Radio frequency driven eseem spectroscopy on spin systems with isotropic hyperfine interactions, J. Chem. Phys. 115 (2001) 10863.
[42] H. Salwen, Phys. Rev. 99 (1955) 1274.
[43] F. Bloch, A. Siegert, Phys. Rev. 57 (1940) 522.
[44] G.N. Watson, A Treatise of the Theory of Bessel Functions, Cambridge University Press, London, 1944.
[45] Y.W. Kim, J. Magn. Reson. 46 (1982) 193.
[46] A. Dulčić, B. Rakvin, J. Magn. Reson. 52 (1983) 323.
[47] H. Sakamoto, T. Takui, K. Itoh, Can. J. Chem. 66 (1988) 3077.
[48] G. Ilangovan, J.L. Zweier, P. Kuppusamy, J. Phys. Chem. B 104 (2000) 4047.
[49] G. Ilangovan, J.L. Zweier, P. Kuppusamy, J. Phys. Chem. B 104 (2000) 9404.
[50] P. Turek, J.-J. André, J. Simon, Solid State Commun. 63 (1987) 741.
[51] I. Gromov, J. Shane, J. Forrer, R. Rakhmatoullin, Y. Rozentzwaig, A. Schweiger, J. Magn. Reson. 149 (2001) 196.
[52] J.H. Burgess, R.M. Brown, Rev. Sci. Instrum. 23 (1952) 334.